

The experimental and theoretical determination of
the thermodynamic properties of melts and glasses
from the system $\text{CaO-MgO-Al}_2\text{O}_3\text{-SiO}_2$

Von der Fakultät für Georessourcen und Materialtechnik
der Rheinisch -Westfälischen Technischen Hochschule Aachen

zur Erlangung des akademischen Grades eines
Doktors der Ingenieurwissenschaften

genehmigte Dissertation

vorgelegt von **M.Sc.**

Jin-Wook Shin
aus Yechon, Korea

Berichter: Univ.-Prof. Dr.rer.nat. Reinhard Conradt
Univ.-Prof. Jochen M. Schneider, Ph. D.

Tag der mündlichen Prüfung: 29. Juni 2004

„Diese Dissertation ist auf den Internetseiten der Hochschulbibliothek online verfügbar“

Berichte aus der Materialwissenschaft

Jin-Wook Shin

**The experimental and theoretical determination of the
thermodynamic properties of melts and glasses from
the system $\text{CaO-MgO-Al}_2\text{O}_3\text{-SiO}_2$**

D 82 (Diss. RWTH Aachen)

Shaker Verlag
Aachen 2004

Bibliographic information published by Die Deutsche Bibliothek

Die Deutsche Bibliothek lists this publication in the Deutsche Nationalbibliografie; detailed bibliographic data is available in the internet at <http://dnb.ddb.de>.

Zugl.: Aachen, Techn. Hochsch., Diss., 2004

Copyright Shaker Verlag 2004

All rights reserved. No part of this publication may be reproduced, stored in a retrieval system, or transmitted, in any form or by any means, electronic, mechanical, photocopying, recording or otherwise, without the prior permission of the publishers.

Printed in Germany.

ISBN 3-8322-3048-3

ISSN 1618-5722

Shaker Verlag GmbH • P.O. BOX 101818 • D-52018 Aachen

Phone: 0049/2407/9596-0 • Telefax: 0049/2407/9596-9

Internet: www.shaker.de • eMail: info@shaker.de

Herrn Prof. Dr. rer. nat. R. Conradt, der mir das Thema gestellt und meine wissenschaftliche Arbeit mit seinem Rat begleitet hat, danke ich sehr.

Besonders bin ich ihm dafür dankbar, dass ich meine Kenntnisse am Werkstoff Glas vertiefen konnte. Er hat mir selbstständige Forschungsarbeit ermöglicht und mich hierdurch gefördert.

Herrn Prof. J. M. Schneider, Ph. D. danke ich für die Übernahme des Korreferats.

Hilfreich war auch das kollegiale Miteinander am Institut für Gesteinshüttenkunde. Hervorheben möchte ich meinen Gruppenleiter Herrn Dipl. -Ing. Wolfgang Wilsmann. Er hat mich durch fachliche Diskussionen und das Lesen der Korrektur unterstützt.

Meiner Frau Hye-Jin und unseren Familien gilt mein herzlicher Dank.

Abstract

The purpose of the present investigation is to illustrate experimental methods for the measurement of accurate thermodynamic data in silicate glasses and melts, and then to determine thermochemical properties by those methods in order to compare with calculated values. Thermodynamic properties of CaO in the melts in the system (CaO-MgO-Al₂O₃-SiO₂) are investigated by electrochemical and calorimetric methods. Activities of CaO are measured in the temperature range 1473 K to 1573 K using EMF measurement. Partial molar mixing enthalpies of CaO are directly measured using isothermal drop calorimetry at 1732 K. The vitrification enthalpy (H^{vit}) of glassy samples was also measured by the isothermal drop calorimeter. The measurements for the vitrification enthalpy were carried out in the temperature range from room temperature T_0 (295 K) to the calorimetric temperature T_k (1732 K). Enthalpy data were determined from the enthalpy difference $\Delta H (T_k - T_0)$. The glass transformation temperature (T_g) and the jump of the heat capacity at T_g (Δc_p) were measured by a dynamic operating calorimeter (DSC). For the sake of the comparison of the experimentally determined activities, two models (F*A*C*T and the constitutional model) are adopted to calculate activities of CaO in the silicate melts. The calculated values agree within ± 0.2 as decadal logarithms with the measured values.

Kurzfassung

Das Ziel dieser Arbeit ist die Erklärung der experimentellen Methoden für die Bestimmung thermodynamischer Größen im glasbildenden Silicatsystem und das Vergleichen dieser experimentell gemessenen Daten mit den berechneten Daten zweier thermodynamischer Modelle. In dieser Arbeit wurden zwei experimentelle Methoden durchgeführt um die thermodynamischen Größen des CaO im Silicatsystem (CaO-MgO-Al₂O₃-SiO₂) zu messen. Mit der EMK-Methode sind Aktivitäten des CaO in Silicatschmelzen im Temperaturbereich von 1473 K bis 1573 K bestimmt worden. Mit einem Einwurfkalorimeter wurde die partiell molar gemischte Enthalpie des CaO bei 1732 K gemessen. Die Vitrificationenthalpie (H^{vit}) der Glasproben wurde ebenso mit dem Einwurfkalorimeter gemessen. Das Experiment wurde im Temperaturbereich von Raumtemperatur T_0 (295 K) bis kalorimetrische Temperatur T_k (1732 K) durchgeführt. Die Glasübergangstemperatur (T_g) und die Wärmekapazitätsdifferenz (ΔC_p) bei T_g zwischen Glas und unterkühlter Schmelze wurden durch den DSC gemessen. Um die experimentell gemessenen CaO-Aktivitäten in Silikatschmelzen zu vergleichen, wurden zwei thermodynamische Modelle ($F^*A^*C^*T$ und das konstitutionelle Modell) für die Berechnung der CaO-Aktivitäten eingesetzt. Die berechneten Aktivitäten stimmen innerhalb ± 0.2 als Logarithmus mit den gemessenen Werten überein.

Contents

1.	Introduction	7
2.	Theory	9
2.1	The glass transition and the glassy state	9
2.1.1	The glass transition	9
2.1.1.1	Phenomenological aspects	9
2.1.1.2	Thermodynamic aspects	11
2.2	Experimental methods in thermochemistry	14
2.2.1	Electrochemical methods	14
2.2.2	Calorimetric methods	17
3.	Experimental	22
3.1	Preparation of glassy samples	22
3.1.1	Selection of compositions	22
3.1.2	Calculation of constitutional compounds	26
3.1.3	Sample preparation	30
3.1.4	Characterization of samples	30
3.2	Determination of CaO activities in the melt	31
3.2.1	Assembly of equipment	33
3.2.2	Description and characterization of the electrolyte	35
3.3	Determination of ΔC_p and T_g by differential scanning calorimeter	45
3.3.1	Description of a dynamic calorimeter	45
3.3.2	Calibration of a dynamic calorimeter	46
3.3.3	Measurement of T_g and ΔC_p	47
3.4	Determination of H^{vt} and ΔH_{CaO}^{mix} by isothermal drop calorimeter	48
3.4.1	Description of an isothermal drop calorimeter	48
3.4.2	Calibration of an isothermal drop calorimeter	51
3.4.3	Measurement of H^{vt} and ΔH_{CaO}^{mix}	54
4.	Thermodynamic modeling	58
4.1	Constitutional model	58
4.2	Modified quasichemical model	63

5.	Results and discussion	68
5.1	Results of calculation and EMF measurement	68
5.1.1	Calculation of oxide activities in the melts	68
5.1.2	Experimental results	71
5.2	Results of calculation and calorimetric measurement	82
5.2.1	Calculation of H^{vit} and $\Delta H^{\text{mix}}_{\text{CaO}}$	82
5.2.2	Experimental results of calorimetric measurement	85
6.	Summary	92
7.	References	95
8.	Appendices	103
8.1	Data for constitutional compounds	103
8.2	Formation enthalpy of constitutional compounds	107

1. Introduction

A quantitative thermochemical description of multicomponent oxide melts is a matter of high interest for both science and technology. Such systems play an important role in metallurgy, glass technology, geology etc. In recent years great progress has been made in applying thermodynamics to technical areas to predict and interpret thermochemical properties of multicomponent systems with the aid of different elaborate models, among which are: the modified quasi-chemical model [PEL 1986], the cell model [GAY 1984], and the model of ideal mixing of complex components [BON 1990].

However, the application of thermodynamics has often been limited by the lack of reliable thermochemical data in multicomponent oxide systems. This is especially true for equilibria involving silicate melts, for which, at present, there are still much less data than for crystalline phases. Although a thermodynamic interpretation of silicate melts was consequential to glass technology, properties of silicate melts have not really been extensively studied by glass industry until the last decade. Liquid silicates, in fact, had been investigated mainly by metallurgists, who long ago perceived the need for more thermodynamic data, in addition to phase diagrams, for a quantitative understanding of phase equilibria involving slags. Nevertheless, through lack of other data, thermodynamic studies of glass-forming silicate systems are of great importance both for the solution of various problems of glass manufacturing and for a more comprehensive understanding of the nature of the vitreous state.

On the basis of thermodynamic information about oxide systems, it is possible to estimate the probability of glass-forming processes and to predict their direction, to determine the durability of the products formed, to calculate the heat balances of reactions and to choose the conditions of glass processing.

Thermodynamic data can also be used to estimate the degree of ordering of the glass structure and to determine the character of the ordering processes occurring in the course of the glass formation. The values of the Gibbs energy of formation determine the extent of rearrangement, which occurs during the fusion, and interaction of oxides forming a glass. Experimental thermodynamic data serve as a criterion for the reliability of statistical models and determine

how to choose the best ones. For elaborated models and databases used in computational thermochemistry, the generation of data for multicomponent silicate melts still is a major problem.

It is the purpose of the present investigation to illustrate experimental methods for the measurement of accurate thermodynamic data in silicate glasses and melts, and then to determine thermodynamic properties by those methods in order to improve the accuracy of the models proposed for calculating in the multicomponent silicate system.

2. Theory

2.1 The glass transition and the glassy state

2.1.1 The glass transition

2.1.1.1 Phenomenological aspects

The classical way to produce glass is to cool a liquid so quickly that crystallization does not have time to occur. As the temperature decreases, the continuous increase of viscosity results in a progressive freezing-in of the liquid to its final rigid condition. To study this process with more precision, it is convenient to follow the evolution of a thermodynamic variable, e.g. the specific volume, V_l as a function of temperature (Figure 2.1 a).

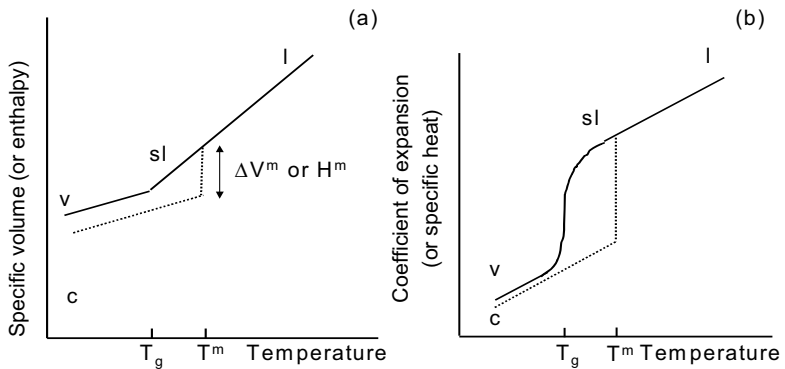


Fig. 2.1 Definition of the glass transition temperature T_g . (a) Variation of the specific volume (or the enthalpy H) with temperature (l: liquid, sl: supercooled liquid, c: crystal, v: glass). (b) Variation of derivative quantities: coefficient of expansion α (or specific heat c_p) [ZAR 1991]

Starting with one-component liquid at an elevated temperature, the lowering of the temperature first causes a contraction. When the melting point T^m is

reached two phenomena may occur – either the liquid crystallizes and a discontinuity ΔV^m (generally a contraction) is introduced in the curve (in reality, a certain degree of undercooling has to be reached to initiate crystallization), or crystallization is avoided and the liquid passes to a supercooled state. In the latter case, the representative point follows an extension of the liquid curve, which passes the temperature T^m without discontinuity. It is as if the system “ignored” the melting point.

In the first case, on completion of crystallization, as the temperature decreases the crystalline solid contracts again, the slope of the curve now is less steep than that of the initial liquid (about 1/3). In the second case, the decrease in the temperature at first causes a contraction of the supercooled liquid with a coefficient of expansion identical to that of the original liquid.

Then, starting at a certain temperature T_g , the slope of the curve decreases to become close to that of the crystalline solid. This break in the cooling curve marks the passage from a supercooled liquid to a glass. The temperature T_g is called the transition temperature or the glass transformation temperature. The viscosity of the liquid increases continuously as the temperature decreases, and the passage through T_g corresponds to a viscosity in the neighbourhood of 10^{13} dPa s. Note that, in contrast to V , the coefficient of expansion α shows a rapid change on passing through T_g (Figure 2.1 b).

At constant pressure, the position of the transition point T_g is not fixed as in the case of T^m but varies slightly with the rate at which the liquid is cooled. Rapid cooling has the effect of shifting the break defining T_g towards higher temperatures while slow cooling displaces T_g towards lower temperatures, as shown in figure 2.2. Bartenev et al. [BAR 1972] have suggested the following formula for the observed transformation temperature T_g as a function of the cooling speed q :

$$q = A \cdot \exp(E_q / RT_g)$$

where E_q denotes activation energies. The values of T_g resulting from different experiments can be slightly different. Therefore, to be completely rigorous in speaking of T_g , it is necessary to define cooling rate and the method used for its determination.

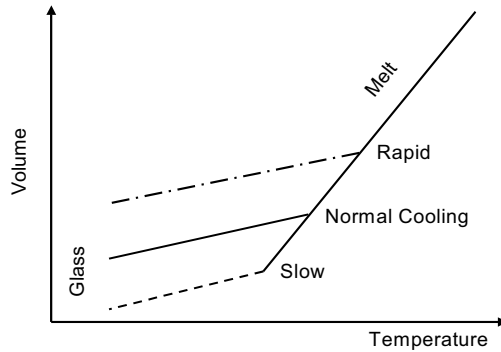


Fig. 2.2 Influence of cooling rate on glass formation [GLA 1990].

2.1.1.2 Thermodynamic aspects

The variations in the specific heat (Figure 2.1 a) are in all respects analogous to those variations in volume already studied with the following exception: the discontinuity H^m corresponding to the latent heat of fusion is always positive while $\Delta V^m = V_l - V_c$ may, depending on the particular case, be either positive or, more rarely, negative (subscripts l and c refer to liquid and crystal respectively).

The specific heat at constant pressure, $c_p = (\partial H / \partial T)_p$ is obtained by derivation from the preceding curves (Figure 2.1 b). As the system vitrifies, the passage through T^m does not show a discontinuity. When c_p diminishes rapidly in the neighbourhood of T_g , the specific heat of the glass tends toward that of the crystal.

The variation of entropy is:

$$dS = \frac{c_p dT}{T} = c_p d \ln T . \quad (2.1)$$

Representing c_p as a function of $\ln T$, the variations in the entropy can be deduced from the areas under the curves.

The specific heat of the liquid, supercooled liquid or glass is designated by c_{pl} , and the specific heat of the crystalline solid is designated by c_{ps} (Figure 2.3).

The entropy of the liquid at a temperature $T > T^m$ is evaluated by integration from absolute zero following first the path crystal \rightarrow liquid:

$$S_l = \int_0^{T^m} c_{ps} \frac{dT}{T} + \frac{H^m}{T^m} + \int_{T^m}^T c_{pl} \frac{dT}{T} \quad (2.2)$$

For the crystal, the entropy at absolute zero is zero following the third law of thermodynamics.

The same value for the entropy of the liquid, S_l must be obtained following this time the path glass \rightarrow liquid:

$$S_l = S^{vit}_{(0)} + \int_0^{T_g} c_{ps} \frac{dT}{T} + \int_{T_g}^{T^m} c_{pl} \frac{dT}{T} + \int_{T^m}^T c_{pl} \frac{dT}{T} \quad (2.3)$$

where $S^{vit}_{(0)}$ denotes the entropy at absolute zero temperature in glass.

By setting the two values of S_l equal, it is possible to deduce the unknown value of the entropy $S^{vit}_{(0)}$ of the glass at absolute zero:

$$S^{vit}_{(0)} = \frac{H^m}{T^m} - \int_0^{T^m} (c_{pl} - c_{ps}) \frac{dT}{T} \quad (2.4)$$

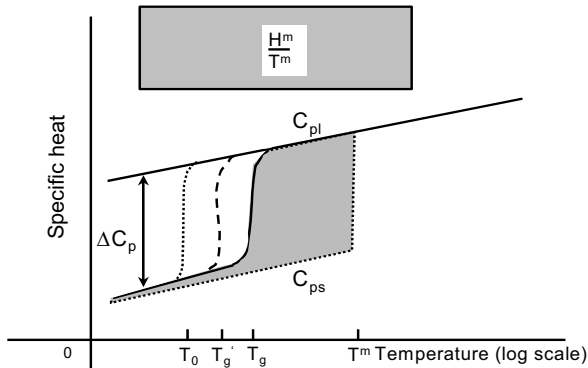


Fig. 2.3 Determination of the excess entropy of a glass. The variation of c_p for a glass cooled more slowly is shown by the dashed line and the dotted line is the extrapolation limit for a cooling rate tending towards zero. The rectangle represents the entropy of fusion of the crystal. [ZAR 1991]

$S^{\text{vit}}_{(0)}$ corresponds to the difference between the entropy of fusion of the crystal and that represented by the shaded area between the two paths shown in figure 2.3. Experiments show that $S^{\text{vit}}_{(0)}$ is not zero, and thus the third law of thermodynamics does not apply to glasses. It is then easy to evaluate the entropy difference

$$\Delta S = S_{\text{liquid or glass}} - S_{\text{crystal}} \quad (2.5)$$

for temperatures $T < T^m$

$$\Delta S = \frac{H^m}{T^m} - \int_T^{T^m} (c_{pl} - c_{ps}) \frac{dT}{T} \quad (2.6)$$

Figure 2.4 shows the variations of ΔS as a function of the temperature. In the course of the transition, the system seeks unsuccessfully to reduce ΔS and some entropy of fusion is retained at T_g . This corresponds to the configurational disorder of the liquid which is frozen in at the moment of glass formation.

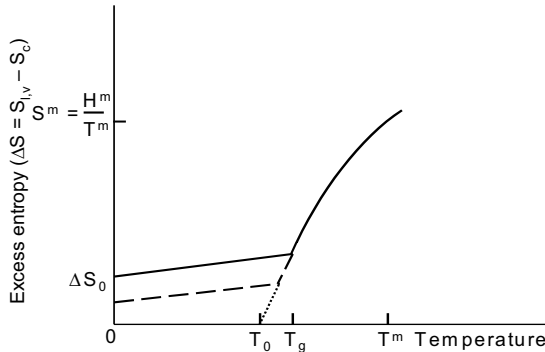


Fig. 2.4 Variation of the excess entropy ΔS with temperature. Dashed line is for a slower cooling rate. [ZAR 1991]

2.2 Experimental methods in thermochemistry

2.2.1 Electrochemical methods

The Gibbs energy of a mixture in general in terms of a homogeneous equilibrium mixture of oxides j is given by the equation

$$G = \sum_j n_j \cdot G_j^0 + RT \sum_j n_j \cdot \ln x_j + G^E, \quad (2.7)$$

here G_j^0 , n_j , and x_j denote the Gibbs energy, molar amount and molar fraction of the pure constituent j , respectively. The second term on the right hand side of (2.7) represents the so-called ideal Gibbs energy of mixing.

$$G^{MX, id} = RT \sum_j n_j \cdot \ln x_j = -T S^{MX, id} \quad (2.8)$$

with entropic contributions due to mere statistical mixing only. Thus, the ideal Gibbs energy of the mixture G^{id} depends on the properties of the pure constituents j and on the stoichiometry of the mixture alone. The properties of a mixture are examined via the concept of excess functions. The excess value of an extensive thermodynamic solution property is simply the difference between its actual value and the value when the solution shows ideal behaviour; e.g., in terms of the Gibbs energy of the solution,

$$G = G^{id} + G^E \quad (2.9)$$

where G = the molar Gibbs energy of the solution,
 G^{id} = the molar Gibbs energy which the solution would have if ideal,
 G^E = the excess molar Gibbs energy of the solution.

The excess term G^E serves as a basis for defining activity coefficients f_j with reference to the pure substances j :

$$G^E = \sum_j n_j \cdot \ln f_j; \quad (2.10)$$

remembering that activities are defined by $a_j = x_j \cdot f_j$.

Activities of oxides may be determined by various methods (e.g., mass spectrometry, electromotive force measurements, phase equilibria and vapor pressure measurements) as a function of temperature and concentration. The electromotive force (EMF) technique is one of the principal methods used for determination of the thermodynamic properties of solutions, molten salts and alloys. In recent decades, this method has been successfully employed for studying oxide glass-forming liquids. The possibility of obtaining complete sets of thermodynamic potentials for these liquids and their components in extended intervals of concentration and temperature constitutes the essential advantage of the EMF technique. The comprehensive information provided by this method often compensates the lack of experimental accuracy by comparison with the accuracy of the calorimetric techniques. In spite of a strong point of the EMF technique, the principle problem, which faces the experimentalist who wishes to apply the EMF technique in order to measure thermodynamic data, is to find a suitable reversible electrolyte for the cell, which is investigated.

The recorded EMF between the two terminals of an isothermal galvanic cell is thermodynamically well defined and can be related to the relevant chemical reactions occurring at the two electrodes by means of Nernst's equation provided the electrode processes satisfy certain conditions. The factors that affect these processes determine the choice of the electrolyte and the electrodes for a particular application.

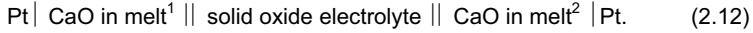
In the majority of studies concerned with silicate melts, the following type of concentration cell is used:



where the solid vertical lines represent the phase boundary between platinum and the melts, whereas the double solid vertical line depicts the boundary

between the solid oxide electrolyte and the melts. In practically all investigations where such cells are employed the electrodes are made of platinum.

Consider a cell in which CaO activity in the silicate system is to be measured. The cell would be represented diagrammatically thus:



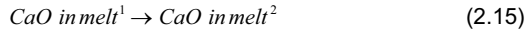
The electrode reactions will then be at the right-hand electrode



and at the left-hand electrode



giving the overall cell reaction



If the electrolyte system conducts electricity by the migration of ions only, then the electrons must move from cathode to anode via an external electronic conductor. It is along this conductor that the electric potential, which is generated by the cell reaction, can be measured. When no current passes through this conductor, the EMF is obtained, the so-called "open-circuit" potential, which is related to the standard Gibbs energy change for the cell reaction by the Nernst's equation.

$$\begin{aligned} E &= -\frac{RT}{2F} \ln \frac{a^1_{\text{CaO}}(\text{melt } 1)}{a^2_{\text{CaO}}(\text{melt } 2)} \\ &= -\frac{1}{2F} (\mu^1_{\text{CaO}} - \mu^2_{\text{CaO}}), \end{aligned} \quad (2.16)$$

Where R is the gas constant, T is the experimental temperature, F is the Faraday constant.

In most practical high-temperature systems the electrolyte usually has a small component of non-electrolytic conduction. A real electrochemical system therefore has a potential, which is given by the equation

$$E = - \frac{RT}{zF} \int_{a_j^1}^{a_j^2} t_i d \ln a_j \quad (2.17)$$

where z is the number of equivalent of charge and t_i is the ionic transport number of the species, which is conducted through the electrolyte having the thermodynamic activity a_j^1 at one electrode and a_j^2 at the other.

2.2.2 Calorimetric methods

To illustrate the need for extensive, accurate thermochemical data in various kinds of thermodynamic models of silicate melts, consider the simple example of the isobaric equilibrium between a melt and a crystal along a liquidus surface. The condition for equilibrium is that the chemical potential μ of the various components be the same in the liquid (l) and crystalline (s) phases, whence, for component j ,

$$\mu_{jc} = \mu_{jl} \quad (2.18)$$

Denoting by μ_j^0 the chemical potential of pure j (at temperature T and pressure P), and by ΔH_j^{mix} and ΔS_j^{mix} the partial molar enthalpy and entropy of mixing, one writes

$$\mu_j = \mu_j^0 + \Delta H_j^{\text{mix}} - T \Delta S_j^{\text{mix}} \quad (2.19)$$

The relationships between the ΔH_j^{mix} , ΔS_j^{mix} , and the measured molar fractions x_j of the selected components that are needed to evaluate (2.19) obviously depend on the thermodynamic model used.

However, $\mu_{jc}^0 - \mu_{jl}^0$ can be written by the calorimetrically evaluated expression, independently, as

$$\mu_{jc}^0 - \mu_{jl}^0 = - \int_T^{T^m} (c_{pc} - c_{pl}) dT + T \int_T^{T^m} \frac{(c_{pc} - c_{pl})}{T} dT + H^m \left(\frac{T}{T^m} - 1 \right) \quad (2.20)$$

where c_p denotes the heat capacity and T^m and H^m denote the temperature and enthalpy of fusion of the pure crystal.

Hence to assess the validity of a thermodynamic model, one must compare the results of the model to those of the calorimetrically evaluated expression (2.20). Without H^m and c_{pc} and c_{pl} data, such an assessment is thus virtually impossible, as discussed in more detail by Bottinga and Richet [BOT 1978].

Equation 2.19 can be rewritten as a function of the activity a as follows:

$$\mu_{jl} = \mu_{jl}^0 + RT \ln a_{jl} \quad (2.21)$$

where R is the gas constant. Equations 2.19 and 2.21 can be used for modeling purposes, and another important point is that, by differentiation of equation 2.21, one also obtains partial molar enthalpies and entropies of mixing:

$$\Delta H_j^{mix} = -T^2 \left[\frac{\partial (\mu_j / T - \mu_{jl}^0 / T)}{\partial T} \right] = -RT^2 \left(\frac{\partial \ln a_j}{\partial T} \right) \quad (2.22)$$

$$\Delta S_j^{mix} = \frac{(\mu_{jl}^0 - \mu_j + \Delta H_j^{mix})}{T} - R \ln a_j - RT \left(\frac{\partial \ln a_j}{\partial T} \right) \quad (2.23)$$

Because enthalpies and entropies of mixing obtained by this way are derivative properties, their accuracy is lower than that of the original activity measurements. The availability of direct, experimental enthalpy of mixing data is thus also valuable. Likewise, by differentiating equation 2.22 one may derive partial molar heat capacities of mixing whose accuracy however is much poorer than that provided by direct c_p determinations. But unfortunately direct c_p measurements in the high temperature are not available. In any case, reliable c_p and H^m data are needed when one uses the activity results for calculating liquid-crystal phase equilibria with (2.20) and (2.21). Fortunately, ΔH_j^{mix} values can be

determined via calorimetric measurements of enthalpies of mixing (ΔH^{mix}), and when they are known, much stronger constraints can be applied to thermodynamic models.

As described in chapter 2.1.1.1, liquids generally transform into crystals on cooling, and this process is accompanied by discontinuities in both first-order and second-order thermodynamic properties (e.g., enthalpy and volume, and heat capacity and coefficient of thermal expansion, respectively). These discontinuities are shown in Figure 2.5 at $T = T^m$ for the enthalpy and heat capacity in the case of one component system. If cooling is fast enough, however, one observes that various liquids supercool, i.e., that crystallization does not occur. On further cooling, one observes eventually a temperature interval where second-order properties decrease markedly without discontinuities in the first-order properties. This interval that separates the liquid from the glassy state is the glass transition range, and the glass transition temperature (T_g) is arbitrarily defined as the temperature at which the extrapolation of the measured properties of the glass and of the liquid intersect. The energetic difference between glass and crystal at absolute zero temperature is accounted for by the heat and entropy of vitrification, H^{vit} and S^{vit} , respectively. These values are maintained in good approximation up to the glass transition temperature T_g [GUT 1995] hence

$$H^{\text{vit}}(0) \approx H^{\text{vit}}(T_g) = : H^{\text{vit}} \text{ also} \quad (2.24)$$

$$S^{\text{vit}}(0) \approx S^{\text{vit}}(T_g) = : S^{\text{vit}}. \quad (2.25)$$

Equations 2.24 and 2.25 imply the relation

$$c_p(\text{s}) \approx c_p(\text{gl}) \text{ for } T < T_g, \quad (2.26)$$

which is an acceptable estimate, except for the low- T c_p excess of glasses (gl) over their corresponding crystals (s) [CHA 1998]. The difference between glass and crystal is also reflected by the value of T_g itself, and by the jump of the heat capacity c_p at T_g ; the jump is approximated by a constant Δc_p given by

$$\Delta c_p \cdot (T^m - T_g) = \int_{T_g}^{T^m} [c_{p,gl} - c_{p,s}] \cdot dT . \quad (2.27)$$

The liquid state at melting temperature T^m serves as a further point of reference. Since it can be reached by heating either the crystal or the glass, the following relations hold

$$H^m - H^{vit} = \Delta c_p \cdot (T^m - T_g) \quad (2.28)$$

$$S^m - S^{vit} = -\Delta c_p \cdot \ln(T_g / T^m) \quad (2.29)$$

Thus, only two among the four non-equilibrium quantities H^{vit} , S^{vit} , T_g , Δc_p need to be known to achieve a fully quantitative description of the glassy state.

In this investigation T_g , Δc_p and H^{vit} , ΔH^{mix}_j were measured by a dynamic operating calorimeter (type DSC 404, Netzsch) and a high-temperature calorimeter (type Multi-HTC-1500, Setaram), respectively.

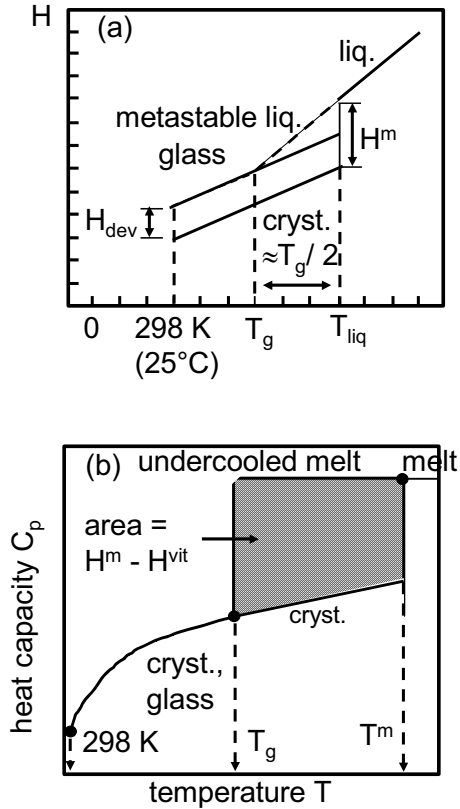


Fig. 2.5 a. Heat content versus temperature of glass forming system, showing the ranges of stable liquid, meta-stable (supercooled) liquid, glass, and crystal; H^m : heat of melting ; H^{vit} : heat of vitrification ; T_g : glass transition temperature ; T^m : melting temperature ; b. Heat capacity versus temperature of glass forming system. [CON 1999*]

3 Experimental

3.1 Preparation of glassy samples

3.1.1 Selection of compositions

The selection of a composition of samples and a system were based on two criteria. First, an amount of data has to exist in the system in order to compare with experimental results and to make a reasonable model. Second, the melting temperature of samples should be below 1300 °C as a matter of corrosion stability. In this investigation, the quaternary system $\text{CaO-MgO-Al}_2\text{O}_3\text{-SiO}_2$ was chosen because this system is fundamental for metallurgy, igneous petrology and glass science. It accounts for more than 90 % of the composition of slags and magmas. For example iron blast-furnace slags can be regarded as consisting of the four major oxide components along with minor proportions of other oxides and of sulfur. Such compositions are also pertinent to mineral fiber glass which have valuable physical and environmental properties. Compositions of samples corresponding to six invariant points were selected in the phase diagram [KOC 1975]. Invariant points like eutectic mixtures have the advantage that melts can be transformed more easily into glass during cooling down and the melting temperature is lower than those around.

Therefore the compositions of the samples were selected at different invariant points in the investigated system. Six samples comprise two samples corresponding to a binary eutectic, one sample to a ternary and three samples to a quaternary eutectic. The compositions of the samples A and B correspond to the binary eutectic in the sub-system anorthite ($\text{CaAl}_2\text{Si}_2\text{O}_8$) - diopside ($\text{CaMgSi}_2\text{O}_6$) and the sub-system anorthite ($\text{CaAl}_2\text{Si}_2\text{O}_8$) - akermanite ($\text{Ca}_2\text{MgSi}_2\text{O}_7$), respectively. That is, for the composition A the oxide composition is 23.5 wt.% CaO, 10.8 wt.% MgO, 15.4 wt.% Al_2O_3 and 50.3 wt.% SiO_2 with the eutectic temperature 1274 °C and sample B has 31.5 wt.% CaO, 8.0 wt.% MgO, 16.9 wt.% Al_2O_3 and 43.6 wt.% SiO_2 with the eutectic temperature 1234 °C. But the composition of sample G corresponds to the ternary eutectic in the sub-system SiO_2 , anorthite ($\text{CaAl}_2\text{Si}_2\text{O}_8$) and wollastonite (CaSiO_3) with 23.3 wt.%

CaO, 14.8 wt.% Al₂O₃, 61.9 wt.% SiO₂ and the eutectic temperature 1170 °C. The compositions and constitutional compounds of the two binary and one ternary eutectic are listed in table 3.1 to 3.3. In the case of the three remaining samples, unfortunately compositions of quaternary invariant points are not known precisely in the CMAS system (figure 3.1). Because of a deficiency of data, compositions of three quaternary invariant points were determined by the aid of the commercial program F*A*C*T [THO 1988]. Constitutional compounds were calculated (see chapter 3.1.2) with determined compositions of invariant points. Compositions and constitutional compounds of three invariant points calculated are listed in table 3.4 to 3.6.

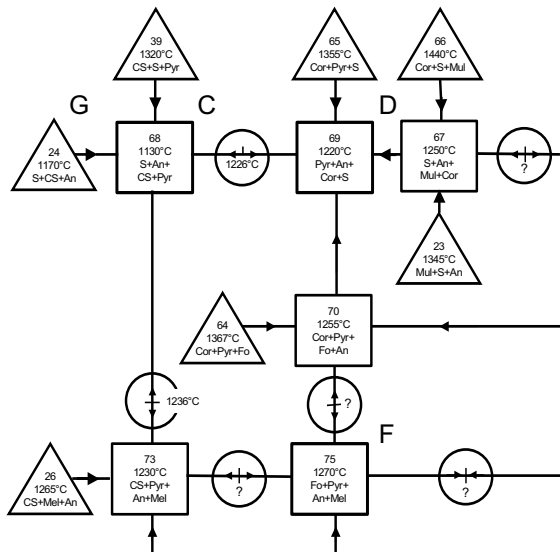


Fig. 3.1 Compositions of samples C to G with reference to constitutional compounds. After [KOC 1975]
 An: anorthite (CaSi₂), CS: wollastonite (CaSiO₃), Cor: cordierite (Mg₂Al₂S₅),
 Pyr: pyroxene (CaMgSi₂-MgSi₂), Mul: mullite (Al₂SiO₅), Fo: forsterite (Mg₂SiO₄),
 Mel: melilite (Ca₂MS₂-C₂AS)

Tab. 3.1 Composition of the eutectic in the system an - an in wt. % in terms of oxide and of constitutional compounds.

Component	T _{liq} (1274 °C)
Oxide:	
CaO	23.5
MgO	10.8
Al₂O₃	15.4
SiO₂	50.3
Phase:	
an	42
di	58

Tab. 3.2 Composition of the eutectic in the system an - ak in wt. % in terms of oxide and of constitutional compounds.

Component	T _{liq} (1234 °C)
Oxide:	
CaO	31.5
MgO	8.0
Al₂O₃	16.9
SiO₂	43.6
Phase:	
an	46
ak	54

Tab. 3.3 Composition of the eutectic in the system an – wol - S in wt. % in terms of oxide and of constitutional compounds.

Component	T _{liq} (1170 °C)
Oxide:	
CaO	23.3
Al₂O₃	14.8
SiO₂	61.9
Phase:	
an	40.4
wol	31.4
S	28.2

Tab. 3.4 Composition of the invariant point C in wt. % in terms of oxide and of constitutional compounds.

Component	INV-C (1138 °C)
Oxide:	
CaO	23.4
MgO	4.3
Al₂O₃	12.8
SiO₂	59.5
Phase:	
S	20.5
wol	21.5
pyr: en_{0.00}-di_{1.00}	23.1
an	34.9
S	20.5
wol	26.6
pyr: en_{0.42}di_{0.58}	18.0
an	34.9
S	20.5
wol	33.9
pyr: en_{1.00}-di_{0.00}	10.7
an	34.9

Tab. 3.5 Composition of the invariant point D in wt. % in terms of oxide and of constitutional compounds.

Component	INV-D (1150 ± 10 °C)
Oxide:	
CaO	11.4
MgO	11.7
Al₂O₃	17.5
SiO₂	59.4
Phasen:	
S	15.6
cor	37.8
pyr: en_{0.00}-di_{1.00}	34.8
an	11.8
S	19.5
cor	0.0
pyr: en_{0.89}di_{0.11}	32.8
an	47.7

Tab. 3.6 Composition of the invariant point F in wt. % in terms of oxide and of constitutional compounds.

Component	INV-F (1163 °C)
Oxide:	
CaO	27.8
MgO	13.7
Al₂O₃	15.4
SiO₂	43.1
Phasen:	
fo	12.1
mel: ak_{0.96}- geh_{0.04}	48.0
pyr: en_{0.00}-di_{1.00}	0.0
an	39.9
fo	7.3
mel: ak_{0.00}- geh_{1.00}	29.8
pyr: en_{0.00}-di_{1.00}	51.1
an	11.8
fo	1.5
mel: ak_{0.00}- geh_{1.00}	35.4
pyr: en_{0.32}-di_{0.68}	57.0
an	6.1
fo	0.0
mel: ak_{0.00}- geh_{1.00}	36.9
pyr: en_{0.38}-di_{0.62}	58.5
an	4.6

3.1.2 Calculation of constitutional compounds

In order to calculate the thermodynamic properties of melts and glasses, an approach was chosen which is based on the calculation of the constitutional compounds from chemical compositions. This calculation is performed within a base of 4 oxides (CaO, MgO Al₂O₃ and SiO₂). The term of constitution refers to the equilibrium state of complete crystallization. Calculation of constitutional

compounds combines the principle of the CIPW norm calculation (see, e.g. PHI 1990), originally used to calculate the normative crystalline phase content of igneous rocks, with a stringent evaluation of the constitutional relations of the predominant ternaries or quaternaries of glass forming systems.

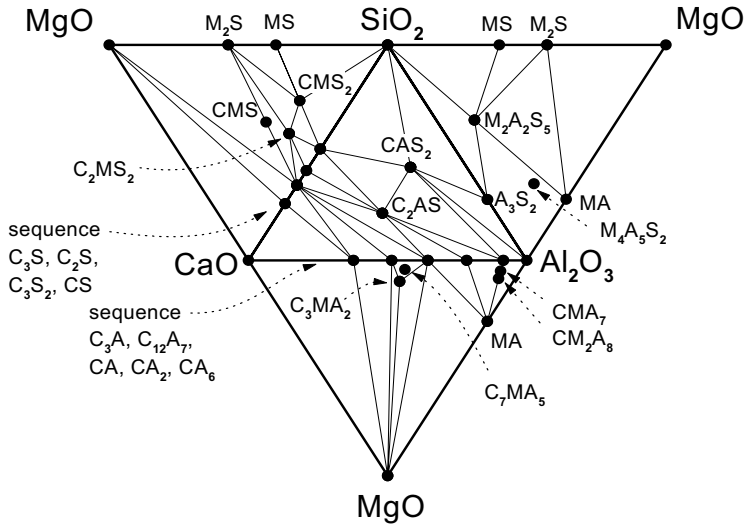


Fig. 3.2 Constitutional compounds in the four ternary systems C-A-S, C-M-S, M-A-S and C-M-A. [CON 2004].

Conradt [CON 1995, CON 1998, CON 1999] modified the CIPW concept for calculating the constitutional compounds of several quaternaries systems, among which are C-M-A-S, N-C-A-S and N-A-B-S ($M = \text{MgO}$, $C = \text{CaO}$, $A = \text{Al}_2\text{O}_3$, $B = \text{B}_2\text{O}_3$ and $S = \text{SiO}_2$), with several minor oxides used in glass application. These predominant systems refer to different glass families, used in conventional glass technology.

The calculation steps were performed by, first, allotting the minor components in the glass, such as P_2O_5 , MnO , La_2O_3 , SrO , TiO_2 , Y_2O_3 or Nd_2O_3 to the most stable co-existing compounds $3\text{CaO}\cdot\text{P}_2\text{O}_5$, $\text{MnO}\cdot\text{SiO}_2$, $\text{La}_2\text{O}_3\cdot\text{SiO}_2$, $\text{Y}_2\text{O}_3\cdot\text{SiO}_2$ and $\text{Nd}_2\text{O}_3\cdot\text{SiO}_2$ etc. Second, the remaining major oxides were allotted to the constitutional compounds by using matrix calculation. According to known

phase diagrams [PHA 1998] the constitutional compounds in the four ternary systems (M-A-S, C-A-S, C-M-S, C-A-M) were determined and shown in figure 3.2. The Short-hand notations C = CaO, M = MgO, A = Al₂O₃ and S = SiO₂ were used. For example, M₂A₂S₅ stands for 2MgO·2Al₂O₃·5SiO₂. Matrix calculation was used to calculate the amount of compounds occurring in the respective constitutional sub-ranges. Figure 3.3 shows an example of the sub-range of co-existing compounds S-CAS₂-MS -CMS₂ in the C-M-A-S system. For example the constitutional compounds at composition c₁ can be calculated from the matrix as can be seen:

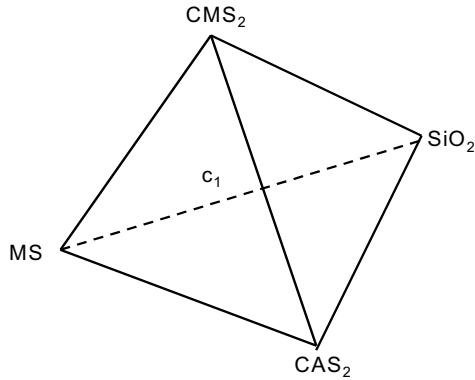


Fig. 3.3 Example of the sub-range of co-existing compounds; S-CAS₂-MS-CMS₂ in the C-M-A-S system

At position c₁:

$$\begin{bmatrix} x_C \\ x_M \\ x_A \\ x_S \end{bmatrix} = \begin{matrix} S & CAS_2 & MS & CMS_2 \\ \begin{bmatrix} 0 & 1 & 0 & 1 \\ 0 & 0 & 1 & 1 \\ 0 & 1 & 0 & 0 \\ 1 & 2 & 1 & 2 \end{bmatrix} \cdot \begin{bmatrix} x_S \\ x_{CAS_2} \\ x_{MS} \\ x_{CMS_2} \end{bmatrix} \\ \begin{bmatrix} x_S \\ x_{CAS_2} \\ x_{MS} \\ x_{CMS_2} \end{bmatrix} = M^{-1} \cdot \begin{bmatrix} x_C \\ x_M \\ x_A \\ x_S \end{bmatrix} \end{matrix}$$

where x_C , x_M , x_A and x_S are the molar fractions of CaO, MgO, Al₂O₃ and SiO₂ respectively.

An example of the constitutional compounds calculation from six different glasses is shown in table 3.7. The results obtained from the constitutional compounds calculation was compared to the results obtained by the commercial software F*A*C*T [BAL 2002] in the table 3.7. F*A*C*T determines the co-existing compounds by a minimum Gibbs energy match to the thermodynamic database. F*A*C*T calculates the crystalline phases during cooling as a function of temperature. The crystalline phases calculated by F*A*C*T in table 3.7 are the phases at room temperature.

Tab. 3.7 Chemical compositions and results of crystalline phases by constitutional compound calculation and by F*A*C*T in wt. %

Glasses	A	B	C	D	F	G
Oxides						
CaO	23.3	31.2	24.6	12.5	27.6	24.6
MgO	10.8	8.1	4.5	11.6	13.8	0.0
Al ₂ O ₃	15.4	16.8	12.6	17.1	15.2	14.3
SiO ₂	50.5	43.9	58.3	58.8	43.4	61.1
Constitutional compound calculation						
CAS ₂	42.02	45.84	34.38	46.66	40.79	39.02
CMS ₂	57.27	2.01	24.17	11.95	-	-
S	0.36	-	17.82	18.04	-	26.31
MS	0.35	-	-	23.35	-	-
C ₂ MS ₂	-	52.12	-	-	46.43	-
M ₂ S	-	0.04	-	-	12.1	-
CS	-	-	23.63	-	-	34.67
C ₂ AS	-	-	-	-	0.68	-
F*A*C*T						
CAS ₂	42.02	45.84	34.38	46.69	40.78	39.15
CMS ₂	57.25	1.61	24.18	11.82	-	-
S	0.21	-	17.81	18.17	-	26.33
MS	0.62	-	-	23.32	-	-
C ₂ MS ₂	-	52.61	-	-	47.14	-
M ₂ S	-	0.04	-	-	11.73	-
CS	-	-	23.63	-	-	34.52
MA	-	-	-	-	0.45	-

3.1.2 Sample preparation

All glass samples were prepared by melting batches from pure α -alumina (Al_2O_3 , 99.99%, Fluka), calcium carbonate (CaCO_3 , Suprapur, Merck), magnesium hydroxide carbonate ($(\text{MgCO}_3) \cdot 4\text{-Mg}(\text{OH})_2 \cdot 5\text{H}_2\text{O}$, p. a., Merck) and silica glass (SiO_2) in a platinum crucible. The powders were mixed in a stoichiometric ratio, and were melted at a temperature of 1550 °C for 4 h and then quenched. This melting process was carried out for a total of two times. Between each melting process, grinding, mixing were conducted for homogenization of samples. After completion of the melting process, glasses were annealed at 800 °C for 4 h and cooled at 3 K/min to room temperature. To confirm the glassy state, all samples were measured by X-ray powder diffraction analyses (XRD). Subsequently, compositions of all glasses were determined from X-ray fluorescence analyses (XFA).

3.1.3 Characterization of samples

Compositions of glass samples were determined by XFA and given in table 3.8.

Tab. 3.8 Composition of glasses A to G in wt.% in terms of oxide

	A	B	C	D	F	G
CaO	23.3	31.2	24.6	12.5	27.6	24.6
MgO	10.8	8.1	4.5	11.6	13.8	0.0
Al₂O₃	15.4	16.8	12.6	17.1	15.2	14.3
SiO₂	50.5	43.9	58.3	58.8	43.4	61.1

For the determination of a vitrification enthalpy (H^{vit}) by the drop calorimeter, samples must be in a glassy state at room temperature. In order to confirm the glassy state, all samples were ground, sieved to less than 63 μm and analysed by XRD. Room temperature X-ray powder diffractometry (XRD) data for all powders were collected with an automated Philips PW3710 instrument using the following standard conditions: Cu-K α -radiation ($\lambda = 1.54056 \text{ \AA}$) produced at 40 kV and 40 mA, 1° divergence for the incident beam and 0.2 receiving slit, goniometer range 5 – 70°, step size = 0.02°. Even though some of the glass

samples showed very weak crystallization peaks as seen in figure 3.4 by X-ray diffraction, all samples can be considered X-ray amorphous.

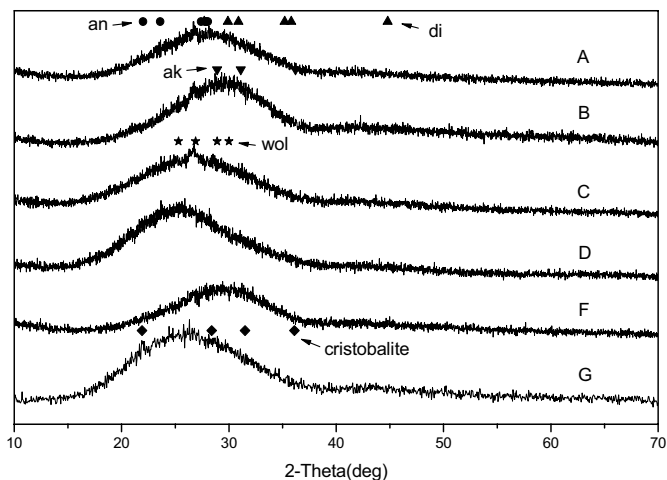


Fig. 3.4 XRD patterns for 6 glassy state samples

3.2 Determination of CaO activities in the melt

The high-temperature solid electrolyte galvanic cells have come into prominence on account of their numerous applications in many thermodynamic and kinetic investigations [SUB 1980]. The growing demand for materials with applications at high temperatures stimulated interest in a systematic investigation of the thermodynamic properties of many oxide systems. Solid-state galvanic cells with a ceramic electrolyte have been found to be highly suitable for these investigations. A significant amount of thermodynamic data pertaining to oxide systems has been collected by this technique. The technique is suitable for the accurate study of quite a number of new oxide systems and non-stoichiometric compounds. The applications of these galvanic cells to the

study of oxide systems are briefly surveyed and an account is given of the systems investigated.

The electrochemical method can be used for the determination of the Gibbs energy change of a reaction. However, the galvanic cell must be so designed as to eliminate all the side reactions, so that the reversible cell potential, E , is related to the Gibbs energy change, ΔG , for the virtual chemical reaction of the cell by the relationship

$$\Delta G = -zFE \quad (3.1)$$

where z denotes the charge valency of ions and F is the Faraday constant. Further, the following relationship has been derived [WAG 1933] for the cell potential E in terms of the ionic transport number, t_{ion} , of the solid electrolyte and the oxygen potential μ'_{O_2} and μ''_{O_2} at the electrodes in case of oxygen-ion-conducting electrolytes

$$E = \frac{1}{4F} \int_{\mu'_{O_2}}^{\mu''_{O_2}} t_{ion} d\mu_{O_2} \quad (3.2)$$

However, the presence of even a small electronic or other ionic contribution to the conductivity will disturb the thermodynamic equilibrium existing at the electrode-electrolyte interface, thereby causing deviations of E from the true EMF. A value of t_{ion} of 0.99 or above is considered to be suitable for most thermodynamic measurements, or, alternatively, the transport number needs to be known.

For the measurement of activity of the CaO in the oxide solution, the following typical galvanic cell can be used:



The EMF of the cell is given by the following equation;

$$E = - \frac{R \cdot T}{2 \cdot F} \cdot \int_{a_{CaO}^{right}}^{a_{CaO}^{left}} t_{Ca^{2+}} d \ln a_{CaO} , \quad (3.3)$$

where $t_{Ca^{2+}}$ is the ionic transport number of CaO, which contribute to a mechanism of an ion conductivity.

Equation 3.3, with the further condition that $t_{Ca^{2+}} = 1$, give:

$$\frac{2 \cdot F \cdot E}{R \cdot T} = \ln a(CaO, right) - \ln a(CaO, left) \quad (3.4)$$

3.2.1 Assembly of equipment

A schematic diagram of the cell assembly used in the present study is given in Figure 3.5. A glass sample was placed in a solid electrolyte crucible attached to an alumina tube. A platinum wire extending from the inner electrode was protected by an alumina capillary and placed inside the alumina tube. The entire sub-assembly described above was placed in a Pt crucible filled with a reference sample. A second platinum wire also protected by an alumina capillary, extended from the Pt crucible. A thermocouple with a Pt/Pt:Rh10 was placed close to the solid electrolyte. The temperature measurement was performed with a digital multi-meter (Type 195 A, $10^9 \Omega$ input resistances, Fa. Keithley) with melting ice as reference. The entire cell assembly was hanged under a stainless steel flange by three alumina tubes and then placed inside a mullite tube (80 mm in O.D., 70 mm in I.D., and 600 mm in height) for protection.

The cell was heated in a vertical resistance tube-furnace with three heating elements, which were controlled with proportion zone, integral time, and differential time (PID) within ± 1 K. A schematic diagram of the furnace used is given in Figure 3.6. The mullite tube with the entire cell assembly was placed inside the furnace on an alumina rod in order to keep in position. The EMF was measured by a high-input impedance electrometer (Type 617, $10^{12} \Omega$ input resistance, Fa. Keithley).

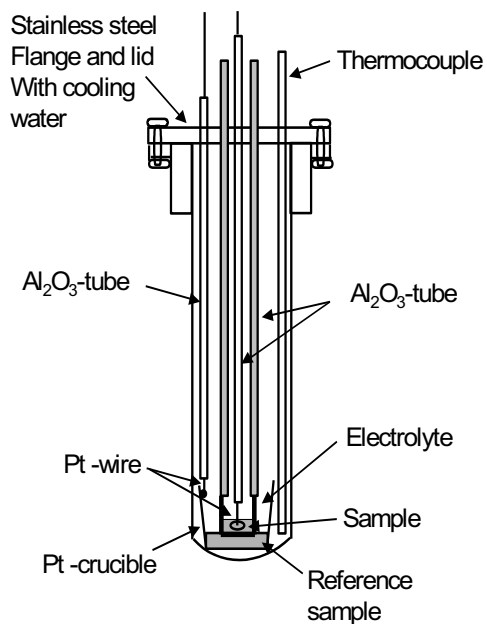


Fig. 3.5 Schematic diagram of the cell assembly for the EMF measurements

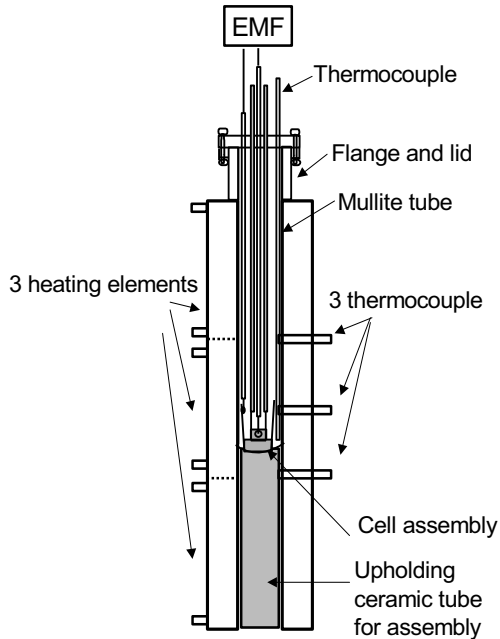


Fig. 3.6 Schematic diagram of the furnace for the EMF measurements

3.2.2 Description and characterization of the electrolyte

There is only one high temperature calcium ion conductor mentioned in the literature, and this is based upon the $\text{CaO-Al}_2\text{O}_3$ system. Calcium β'' -alumina can be prepared by ion-exchange from sodium β'' -alumina [DUN 1980], [WHI 1985] or by direct synthesis from an oxide-based precursor [KUM 1985], [HON 1987], [SCH 1990]. Kirchenerova et al. [KIR 1991] have found that the ion-exchanged calcium β'' -alumina is thermally unstable at elevated temperatures and transforms to calcium magnetoplumbite, which has a structure very similar to that of the β'' -alumina. From this they have concluded that direct synthesis of calcium β'' -alumina is not possible. Structurally this investigation may be of importance, but because calcium magnetoplumbite has a high ionic conductivity, this phase is equally attractive for its use in thermodynamic

measurements. Therefore two kinds of solid-state calcium ion conductor were prepared to measure activities of CaO in silicate melts in the present study. One is calcium β "-alumina based upon sodium β "-alumina and another is calcium magnetoplumbite ($\text{CaO}\cdot 6\text{Al}_2\text{O}_3$) synthesized.

For calcium β "-alumina prepared by ion exchange, commercial sodium β "-alumina tubes, 15mm in O.D., 13mm in I.D., and 40mm in height (Ionotec Ltd, Cheshire WA7 1TQ, England) were used in this experiment as the precursor material. Sodium β "-alumina can be ionically exchanged by immersion in an appropriate molten salt, and the degree of exchange can be monitored by the change in weight. A two-step exchange process was employed for preparing calcium β "-alumina, because the extent of the ion-exchange ratio when preparing calcium β "-alumina directly from sodium β "-alumina is negligible. Thus silver ion exchange was initially employed as an intermediate step. Polycrystalline silver β "-alumina was obtained by ion exchange of sodium β "-alumina in a large excess of molten silver nitrate (AgNO_3). The exchange processes were performed in a α -alumina crucible filled with silver nitrate at a temperature of 300 °C for 24 h. After the ion exchange, the silver β "-alumina was washed in distilled water and anhydrous ethanol to remove the excessive salt; finally it was dried and weighed.

The silver β "-alumina was subsequently immersed in the eutectic mixture of calcium chloride – calcium nitrate ($\text{CaCl}_2\cdot\text{Ca}(\text{NO}_3)_2$), at a temperature of 500 °C for 24 h. Afterwards, it was also washed in distilled water and anhydrous ethanol, and then subsequently dried and weighed. This ion exchange was repeated with the molten salt until no further change in weight was observed. After each ion exchange, the β "-alumina was controlled by X-ray diffraction analysis. The stability of the ion-exchanged β "-alumina was investigated by heating up to a temperature of 1300 °C for 3 h. After this heat treatment, β "-aluminas were analysed by X-ray diffraction.

The degree of ion exchange in commercial sodium β "-alumina was determined gravimetrically by weighing the β "-alumina tubes before and after exchange. After the first step in ion exchange ($\text{Na}^+ \rightarrow \text{Ag}^+$), the degree of ion exchange was 79.8 % according to 27 individual experiments. After the second step ion

exchange ($2\text{Ag}^+ \rightarrow \text{Ca}^{2+}$), the degree of ion exchange was 90.8% according to 15 individual experiments. The ratio of sodium ions remaining in calcium β'' -alumina is 20.2%, and that of silver ions is 7.3%. The result of the ion exchange on sodium β'' -alumina is listed in table 3.9.

Tab. 3.9 Degree of ion exchange in sodium β'' -alumina

	Start	After 1st exchange	After 2nd exchange
Na ₂ O	0.175 mol	0.035 mol	0.035 mol
Ag ₂ O	0.000 mol	0.140 mol	0.014 mol
CaO	0.000 mol	0.000 mol	0.126 mol
degree of ion exchange corresponding to step		79.8 %	90.8 %
degree of ion exchange corresponding to start		79.8 %	72.0 %
mass in g	100	123.7 ± 0.1 (27)	101.2 ± 0.7 (15)

The XRD pattern of the various β'' -alumina is presented in figure 3.7.

As in the case of silver β'' -alumina, the XRD peaks of this material resembled the pattern of its precursor sodium β'' -alumina. However, as can be seen, the XRD peaks of calcium β'' -alumina can be distinguished from those of sodium, silver β'' -alumina by their intensity. Every β'' -alumina was annealed at 1300 °C for 3 h and controlled by X-ray diffraction analysis. After annealing, the XRD peaks of thermally treated silver, calcium β'' -alumina showed the same pattern as that of the magnetoplumbite phase in figure 3.9, while the pattern of sodium β'' -alumina showed no difference. By comparison to sodium β'' -alumina, the calcium- silver β'' -alumina seem to be related to the magnetoplumbite phase and transform to the magnetoplumbite structure at elevated temperatures. As stated above, it is probably due to the low thermal stability of calcium- silver β'' -alumina.

In order to check for the effects of non-exchanged ions, the EMF measurements were carried out in the system CaO and CaO-6Al₂O₃ at a temperature range from 1200 K to 1500 K using partially ion-exchanged calcium β'' -alumina solid electrolyte. Kumar and Kay [KUM 1985] reported that the standard molar Gibbs

energies of formation of the calcium aluminates from the oxides were measured using a calcium β'' -alumina synthesized by solid-state high temperature reactions from CaCO_3 , MgCO_3 and $\alpha\text{-Al}_2\text{O}_3$.

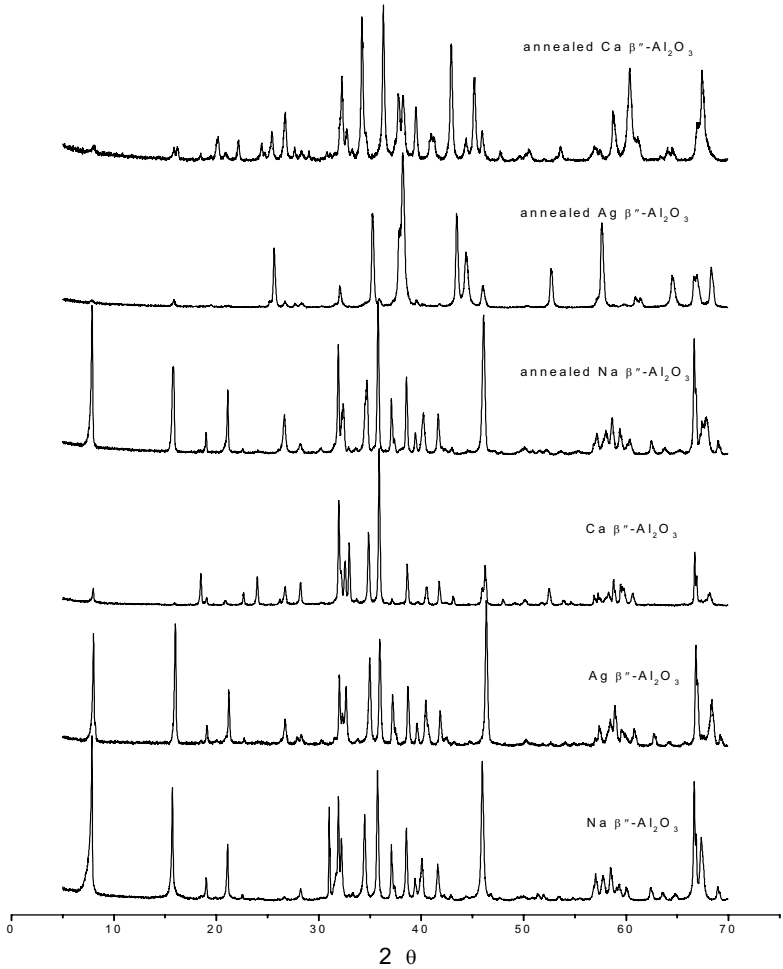


Fig. 3.7 XRD patterns of Na, Ag, Ca β'' -alumina and annealed at 1300 °C for 3 h

In addition, Róg et al. [ROG 1993] measured also the Gibbs energy of formation of calcium aluminates using a completely ion-exchanged calcium β "-alumina prepared by a one step ion-exchange from sodium β "-alumina. None of the above-mentioned studies refer to the effects of the influence by not completely exchanged ions on EMF measurements using a calcium β "-alumina prepared by ion exchange method.

The calcium aluminate, $\text{CaAl}_{12}\text{O}_{19}$, was prepared from pure α -alumina and reagent grade calcium carbonate powders. The powders were mixed in a stoichiometric ratio and subsequently heated up to a temperature of 1200 °C for 60 h for a total of three times. The samples were ground, mixed and X-ray analyzed after each heating cycle. Finally the mixtures were sintered for 6 h at 1600 °C, and the formation of the calcium aluminate $\text{CaAl}_{12}\text{O}_{19}$ was confirmed by X-ray diffraction analysis.

The half-cell mixture was prepared as follows:

A homogeneous mixture of pure CaO and Pt powders in a ratio of 1:2 by weight was prepared as anode material and then placed inside a platinum crucible. A homogeneous mixture of $\text{CaAl}_{12}\text{O}_{19}$ and Al_2O_3 , Pt powders were prepared as cathode material and placed inside the calcium β "-alumina. Then this cathode sub-assembly with calcium β "-alumina was placed on the anode powder. The calcium β "-alumina containing cathode powder was pressed by the Al_2O_3 tube in order to contact with the anode powder of CaO and Pt. So the cell can be represented diagrammatically as

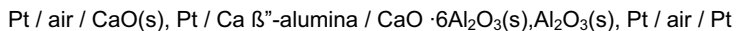


Figure 3.8 shows the EMF vs. temperature plots of the above cell reaction.

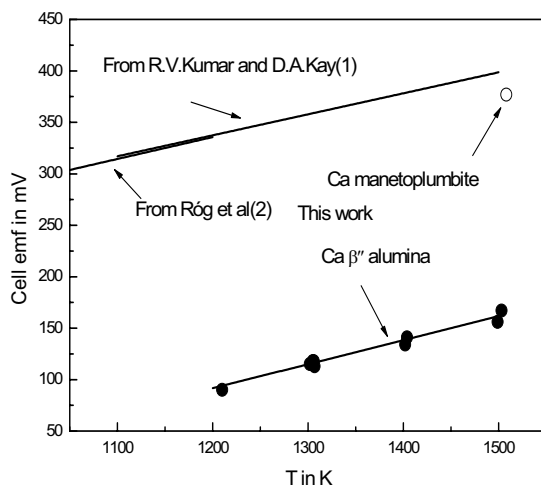


Fig. 3.8 Variation of EMF with temperature for the cell using partially ion-exchanged calcium β'' -alumina and calcium magnetoplumbite in comparison with the literature values

The presented results are compared with the results received by Kumar, and by Róg by solid-state synthesized Ca β'' -alumina without sodium and silver ions. The slope (0.233 mV/K) of the linearized EMF measured in this work is similar to that (0.204 mV/K) obtained by Kumar and Kay in the temperature range from 1100 K to 1500 K. The results are also compared with the literature values measured by the complete ion-exchanged calcium β'' -alumina. Also, in this case, the rate of EMF increase is similar to that (0.213 mV/K) from Róg et al. in the temperature range from 1000 K to 1200 K. But the EMF values obtained from this experiment differ by less than a half of those from the literature. This difference is caused by the not completely exchanged sodium (20.2%) and silver (7.3%) ions in the Calcium β'' -alumina, hence, by Ca value smaller than unity.

The EMF measurement was carried out continuously in the system CaO and CaO·6Al₂O₃ using calcium magnetoplumbite solid electrolyte, which has no

effects of the residual ions on EMF measurements. Since calcium magnetoplumbite is not a compound with a fixed composition, the relevant section of the CaO-MgO-Al₂O₃ ternary system was investigated to determine the extent of the calcium magnetoplumbite phase field. The first step in this investigation consisted in the preparation of oxide mixtures with selected compositions in the relevant portion of the ternary phase diagram. The starting materials CaCO₃, MgCO₃, and α-Al₂O₃ were thoroughly mixed in the selected proportions, calcined and ground at least three successive times, and sintered at 1650 °C for at least four hours. The phases present after sintering were identified by X-ray powder diffraction and given in figure 3.9. The initial compositions of the mixtures and the final phases produced by sintering are given in table 3.10. The magnetoplumbite structure was detected in all cases of XRD investigations on 5 sintered powder samples. But as the amount of magnesium oxide increases, a second phase namely CaO·2Al₂O₃ or 3CaO·Al₂O₃, respectively, was also detected. As the amount of magnesium oxide is 0.8 mol %, spinel phase (MgO·Al₂O₃) was identified.

Tab. 3.10 Synthesis of calcium magnetoplumbite by sintering at 1650 °C for four hours

Molar Proportions			Phases
CaO	Al ₂ O ₃	MgO	
1.0	6.0	0.0	CaO·6Al ₂ O ₃ + α-Al ₂ O ₃
1.0	6.0	0.3	CaO·6Al ₂ O ₃ + CaO·2Al ₂ O ₃
1.0	6.0	0.5	CaO·6Al ₂ O ₃ + 3CaO·Al ₂ O ₃
1.0	6.0	0.7	CaO·6Al ₂ O ₃ + 3CaO·Al ₂ O ₃
1.0	6.0	0.8	CaO·6Al ₂ O ₃ + CaO·2Al ₂ O ₃ + MgO·Al ₂ O ₃

The difference between the measured EMF value using calcium magnetoplumbite synthesized in this work and the value from Kumar and Kay does not exceed 20 mV for the above cell reaction at temperature 1508 K (see figure 3.8). That means it is not greater than a few percent of the measured EMF. From the comparison of both measured EMF values it can be supposed

that the calcium magnetoplumbite has the ionic transport number of CaO ($t_{\text{Ca}^{2+}}$) with the condition that $t_{\text{Ca}^{2+}} \approx 1$. On account of this fact calcium magnetoplumbite ($\text{CaO} \cdot 6\text{Al}_2\text{O}_3$) was used as a solid electrolyte for the measurement of CaO activities in silicate melts.

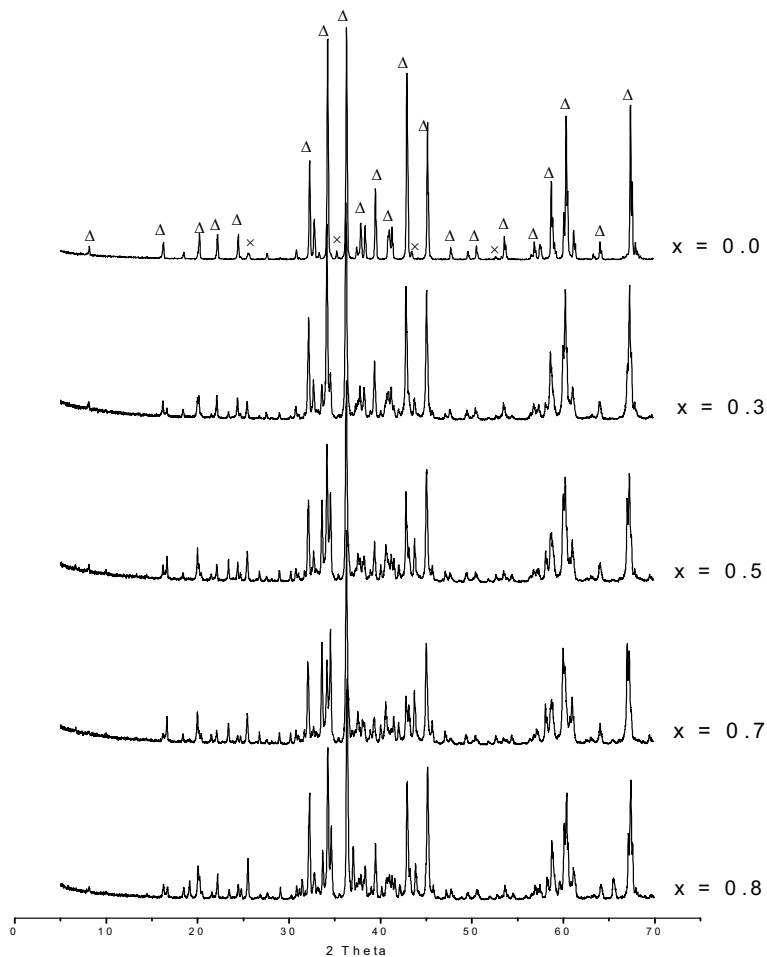


Fig. 3.9 XRD of CA_6M_x synthesized by sintering at 1650 °C for 4 h
(Δ : $\text{CaO} \cdot 6\text{Al}_2\text{O}_3$, x: $\alpha\text{-Al}_2\text{O}_3$)

If the silicate studied is molten at the temperature of investigation, the use of a solid electrolyte tube or crucible makes it possible to separate the reference electrode from the melt. The selection of a suitable container is a major problem, since not all solid electrolytes are available in the form of tubes. The cell has to be designed in such a way as to hold the silicate melt. In order to measure activities of CaO in silicate melt, the solid electrolyte has to exist in the form of a crucible. On that account calcium ion conductors were prepared in the form of a crucible by slip casting. Slip casting is a suitable consolidation process to obtain materials with high green densities and micro structural homogeneity allowing the manufacture of components with complex shapes. Slip casting has been used also for many years in the production of conventional ceramics. For calcium ion conductors prepared by slip casting, a commercial calcium magnetoplumbite powder (Alcoa Super Lightweight Aggregate SLA-92) was used in this experiment as the precursor material.

Aqueous slips were prepared from the calcium magnetoplumbite powder, deionized water as medium, PVA as binding agent, CE64 as deflocculant and anti-foaming agent. For the EMF measurement, solid electrolyte crucibles, 17 mm in O.D., 1 mm in thickness and 16 mm in height, were prepared. Before grinding, raw materials (calcium magnetoplumbite powder: 100 g, deionized water: 60 g, binding agent: 2 g, deflocculant: 1 g, anti-forming agent: 0.3 g) were mixed in a ball mill, then ground for about 24 h. After that, a slip was prepared and cast into plaster moulds (plaster of paris at a gypsum to water ration of 70 %). The objects were dried in air for 1 day and then sintered at 1650 °C for 6 h. The process of the slip casting is presented in figure 3.10 as a flow chart.

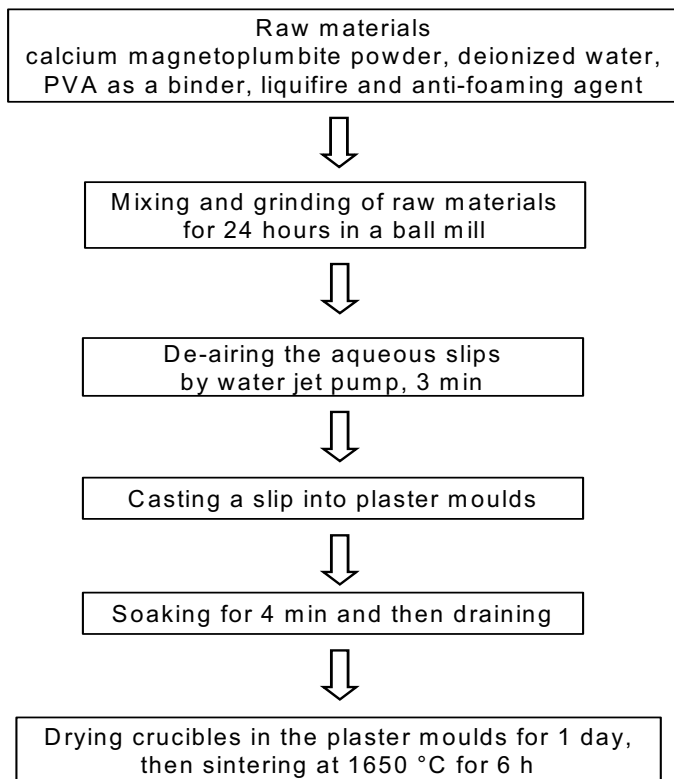


Fig. 3.10 Flow sheet of the process of the slip casting

3.3 Determination of ΔC_P and T_g

Differential Scanning Calorimeter (DSC) instruments are employed to determine not only the glass transition temperature (T_g), but also the difference of heat capacity between undercooled melt and crystal (ΔC_P). In figure 3.11 a dynamic calorimeter (Type DSC 404, Netzsch) used in this investigation is illustrated.

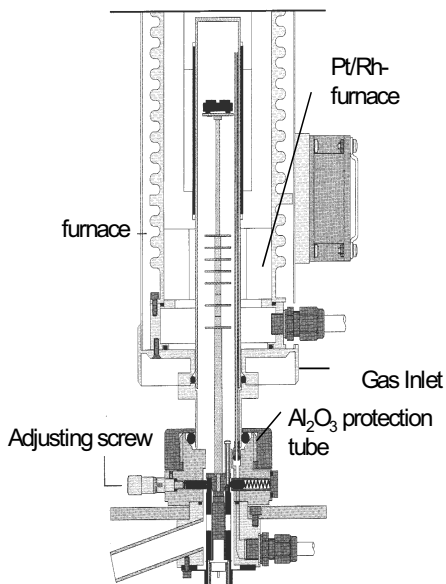


Fig. 3.11 Construction of the dynamic calorimeter (Type DSC 404, Netzsch)

3.3.1 Description of a dynamic calorimeter

A sensor of the dynamic calorimeter consists of a sample holder and heat-sensitive plate. The adjustable sample holder is placed in the center of an Al₂O₃ protection tube, which is enclosed by a Pt/Rh furnace. The sample is encased in a Pt crucible ($\varnothing 6.3 \times 5$ mm), which is placed on one side of the holder, and an empty Pt crucible as reference is likewise placed on the other side of the holder during experiments. The temperature difference between the sample and reference is measured by thermocouples, attached to the base of each side of the holder, as a function of the furnace temperature. The entire measuring head of the dynamic calorimeter is shown in figure 3.12.

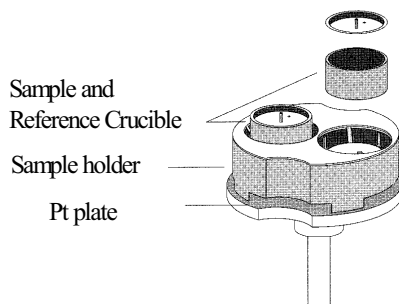


Fig. 3.12 The entire measuring head of the dynamic calorimeter

3.3.2 Calibration of a dynamic calorimeter

Calibration factors of the instrument must be determined because the measured value of temperature and enthalpy for the same transition or reaction depends on the instrument and the experimental conditions, e.g. sample mass, heating rate, shape and material of the container and packing mode. For the employment of the dynamic calorimeter, calibration measurement for the enthalpy and temperature was carried out in this investigation.

A set of materials adopted in this work for the calibration is listed with the values of phase transition points and enthalpies in table 3.11. Accordingly, a known amount of material about 20 mg is scanned in a differential scanning calorimeter operation under fixed conditions. On the basis of the area under the peak, the calibration factor, K (in cm^2J^{-1}) can be determined. Knowing K , we can determine the enthalpy values for other unknown materials.

Tab. 3.11 Phase transition temperatures and enthalpies of calibration reference materials

compound	KClO_4	Ag_2SO_4	SiO_2	BaCO_3	SrCO_3
transition point $^\circ\text{C}$	300.8	426.8	571.0	808.0	928.0
enthalpy of transition J/g	-101.55	-50.32	-12.12	-95.41	-135.20

The heat of transition of a sample can be expressed as follows when it is determined by DSC:

$$\Delta H = \frac{1}{m} \int_{t_e}^{t_f} (dQ/dt) dt \quad (3.5)$$

where ΔH is the transition enthalpy, m sample mass, t time, dQ/dt heat flux difference and subscripts e and f represent the extrapolated onset and final point of the peak, respectively. If the left-hand side of equation 3.5 is considered as ΔH_{ref} (ref = reference) and the right-hand side as ΔH_{meas} (meas = measured), both sides can be equalized by introducing a proportionality factor, K , to give

$$\Delta H = \frac{K}{m} \int_{t_e}^{t_f} (d\tilde{Q}/dt) dt \quad (3.6)$$

where $d\tilde{Q}/dt$ is the amount of heat flux difference in yet uncalibrated units.

For calibration,

$$K = \Delta H_{\text{ref}} / \Delta H_{\text{meas}} \quad (3.7)$$

must be determined. The calibration can be carried out using materials the transition enthalpies of which are well established.

Calibration factors in the form of a polynomial were determined by using 5 compounds in the temperature range 0 – 950 °C. The experiments were conducted under the following conditions: Netzsch type DSC 404, Pt pan, sample size 20 – 25 mg, heating rate 15 K/min in the air.

3.3.3 Measurement of T_g and Δc_p

The experiments for 6 glassy state samples were performed under the same conditions for the determination of calibration factors of DSC. In order to distribute samples homogeneously in the Pt crucible, glass powders were prepared by grinding, sieving less than 63 μm . A bottom of the Pt crucible was covered with the powder sample about 20 mg and then pressed by stamping.

The entire Pt crucible with the lid was placed in one side of the holder, and a same empty Pt crucible was placed in the other side of the holder as reference. Then the investigation was conducted in the air in the temperature range 40 – 1300 °C with a heating rate 15 K/min.

The method of measuring the glass transition temperature and the jump of the heat capacity Δc_p at T_g is outlined in figure 3.14. The glass transition temperature was determined by extrapolating the onset temperature. T_g is the temperature at which the extrapolated baseline before the transition intersects the tangent drawn at the point of greatest slope of the step of the glass transition. The jump of the heat capacity Δc_p was determined by comparing of a deflection of the baseline observed at the glass transition temperature as sketched in figure 3.13.

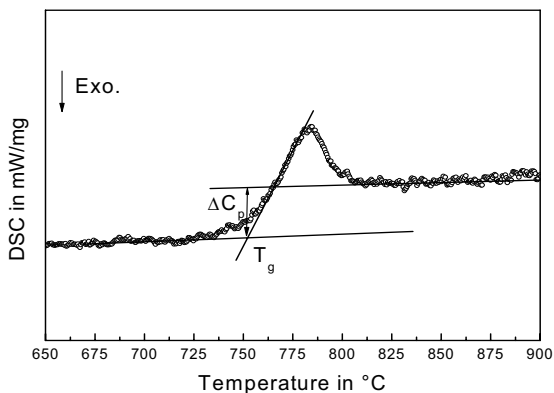


Fig. 3.13 Determination of the glass transition temperature and the jump of the heat capacity Δc_p

3.4 Determination of H^{vit} and $\Delta H^{\text{mix}}_{\text{CaO}}$ by isothermal drop calorimeter

3.4.1 Description of an isothermal drop calorimeter

Calorimetric measurements were made by the drop-mixing method. A set of samples comprising six vitreous samples and well-defined mechanical mixtures

of pure oxides with identical composition, or pure CaO, were dropped at room temperature into the calorimeter operating at 1732 K. The enthalpic effects associated with the reactions occurring in the calorimeter were measured.

All calorimetric experiments were performed in a differential high-temperature integrated heat flux calorimeter. This apparatus is produced by Setaram in France and is available commercially under the designation "Multi Detector High-Temperature Calorimeter".

The grooves on the outside surface of the grooved tube, the charging tube through which samples are dropped into the working crucible, and the lid closing this crucible are not shown. The ceramic parts of the calorimetric detector are made from recrystallized α -alumina [WIL 1989].

The central part of the new calorimeter is represented by the "grooved tube" (length 80 mm; O.D. 20.1 mm; I.D. 17.5 mm) shown in figure 3.14, made from recrystallized alumina. In the wall of the tube, 60 grooves (width 0.5 mm; depth 0.5 mm), cut equidistantly from the outer surface, run parallel to the longitudinal axis. The grooves serve to accommodate the leads of a thermopile, as described below.

A disc-shaped piece of alumina fixed in the middle of the grooved tube by an alumina bolt divides the space enclosed by the tube into two halves. The upper half, acting as the "working cell" of the differential calorimeter, contains the "working crucible" (I.D. 16.5 mm) in which the sample reacts during a calorimetric measurement. The lower half represents the "reference cell" of the calorimeter and holds the "reference crucible". In the calorimetric measurements performed in the course of this study, both the working and reference crucibles were lined by a platinum crucible in order to protect the alumina working crucible from attack by the samples and to maintain a constant and uniform temperature in the reference cell.

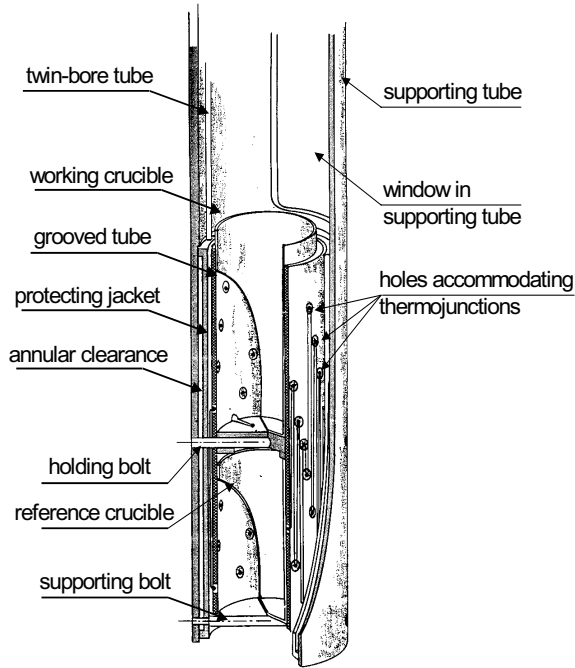


Fig. 3.14 Diagrammatic representation of the detector employed in the Setaram Multi-Detector High-Temperature Calorimeter.

Samples are introduced from the outside into the working cell through an alumina tube ("charging tube" not shown in figure 3.14) projecting into the working crucible. By means of the supporting tube, the calorimeter is suspended in an alumina tube (I.D. 23 mm), which is in turn surrounded by a graphite tube; this tube system is mounted in a water-cooled vacuum jacket. The graphite tube acts as a heating element, which, due to its special profile, allows a zone of constant temperature to be established around the detector.

In order to process the data obtained during the calorimetric measurements (the voltage of the thermopile and that of the thermocouples measuring the calorimeter and furnace temperatures), the microprocessor-operated Setaram G 11 controller is first employed; this amplifies, digitizes, and, finally transfers the data via an RS 232 series interface to an IBM compatible computer which

evaluates the information provided by the measurements. The Setaram G 11 controller is also used to control the furnace temperature, while thyristors are employed to adjust the electric power fed into the graphite heating tube. The electric power is stabilized by an electronic AC voltage stabilizer (Philips PE 1605). The assembly is shown in figure 3.15.

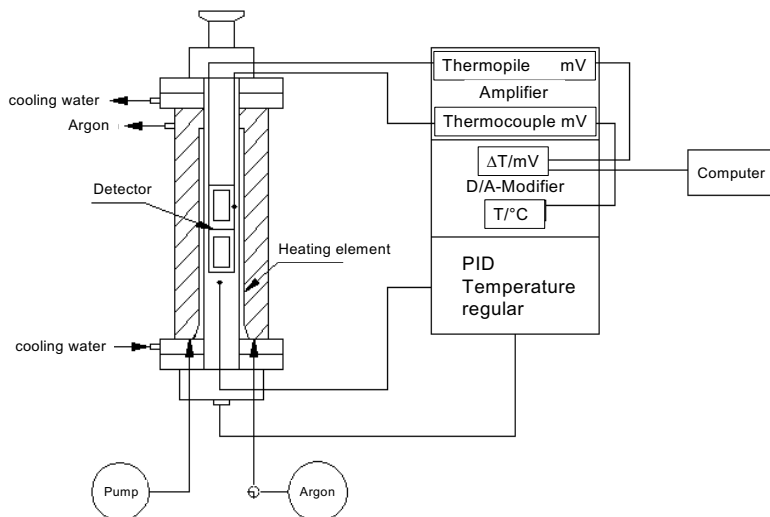


Fig. 3.15 Principal structure of the drop calorimeter periphery

Before initiating an experiment, the vacuum jacket accommodating the calorimeter chamber and the heating element is evacuated by a rotary pump (0.1 Pa), and during a measurement, it is flushed with argon gas (purity; 99.9998 vol.-%). Flow controllers keep the flow rates of the flushing gas and of the water used for cooling the vacuum jacket at fixed values of $3 \text{ cm}^3/\text{s}$ and $25 \text{ cm}^3/\text{s}$, respectively; these had been proved to be optimum values in test runs.

3.4.2 Calibration of the isothermal calorimeter

The calorimeter is calibrated by the drop method: Spheres of platinum at room temperature are dropped into the calorimeter operating at the measurement

temperature. The masses of the spheres are chosen so as to produce heat effects, which are as similar in magnitude as possible to the heat effect of the corresponding reaction run. The calibration factor, f , is calculated from the relation,

$$f = \frac{\Delta H}{I} \quad (3.8)$$

The enthalpy change, ΔH , which the calibration sample experiences in the calorimeter, is calculated from the mass, the initial temperature (= room temperature), and the final temperature (= calorimeter temperature) of the sample using enthalpy data tabulated in the literature [KNA 1991] for platinum, while the value of the integral I , corresponding to ΔH , is provided by the computer in arbitrary units. Thus in the following, f will also be given in J per arbitrary units (a. u.).

The suitability of the differential calorimeter for measurements at high temperatures has been tested using the method of drop calorimeter. In the following, exemplary results characterizing the main features of the calorimeter are presented. In a first series of measurements, the enthalpy difference of α -alumina (sapphire) was determined from room temperature (295 K) to calorimeter temperature (1732 K), platinum being used for calibration in order to obtain information on the accuracy of the calorimetric data. Platinum spheres with masses between 100 and 150 mg were dropped from room temperature into the working cell with the platinum crucible operating at a fixed calorimeter temperature. From the data thus obtained, the calibration factor was calculated according to equation 3.8. Typical results for a calorimeter temperature of 1732 K are presented in figure 3.16. According to the information shown in figure 3.16, the calibration factor is constant and independent of the magnitude of the heat effects produced in the working cell. The deviation of the individual values from the mean value is less than $\pm 3\%$.

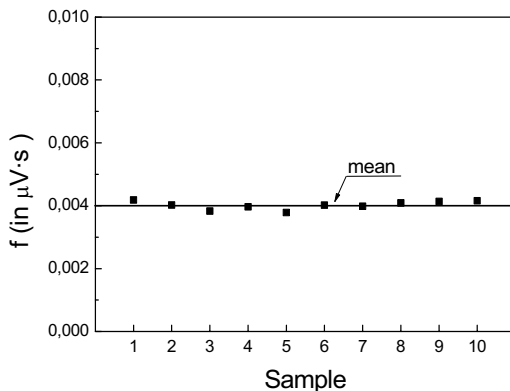


Fig. 3.16 Calibration factor f determined at 1732 K from the individual platinum samples

α -alumina (sapphire) with masses between 10 and 15 mg were dropped also from room temperature into the working cell with the platinum crucible operating at a fixed calorimeter temperature. The enthalpy H (referred to 295 K) of α -alumina at calorimeter temperature (1732 K) was calculated from the enthalpy effects in the working cell using the calibration factor of the platinum. In Table 3.12 the results are compared to data from literature. The deviation of the measured values from the tabulated data is less than $\pm 0.5\%$.

Tab. 3.12 Thermal enthalpy H (referred to 295 K) of α -alumina at 1732 K. Comparison of values (H^1), measured in this study with data (H^2), tabulated in the literature [KNA 1991] and deviation $\delta = 100 (H^1 - H^2)/H^2$.

T in K	H^1 in kJ/mol	H^2 in kJ/mol	δ in %
1732	172.7 ± 1.73 ⁾ (12) ⁺⁾	173.4	-0.4

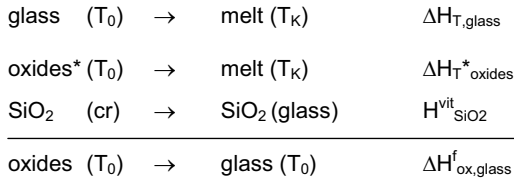
⁾ standard deviation

⁺⁾ number of individual measurements

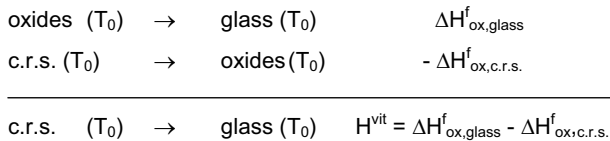
3.4.3 Measurement of H^{vit} and $\Delta H^{\text{mix}}_{\text{CaO}}$

In a series of experiments, vitrification enthalpies (H^{vit}) of six samples described in chapter 3.1.1 were determined by drop calorimeter. In order to determine vitrification enthalpies, two kinds of samples were prepared: glassy sample and pure oxide mixtures with identical composition, respectively.

Calorimetric measurements for the determination of vitrification enthalpies were carried out in the temperature range from room temperature T_0 (295 K) to the calorimetric temperature T_K (1732 K). Enthalpy data were determined from the enthalpy difference ΔH ($T_K - T_0$) between room temperature and calorimeter temperature T_K . The formation enthalpy of glass from the oxides $\Delta H^f_{\text{ox}}(\text{glass})$ can be derived from the directly measured enthalpy difference with the following scheme:



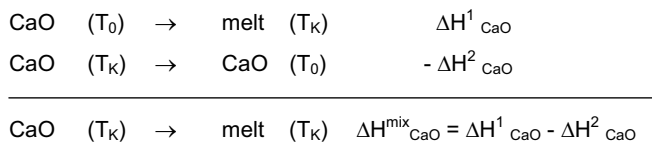
Because silica glass was used as pure silicon oxide at the measurement of oxide mixtures, an amount of vitrification enthalpy of silicon oxide, $H^{\text{vit}}_{\text{SiO}_2}$, must be summed to derive the formation enthalpy of glass from the oxides $\Delta H^f_{\text{ox, glass}}$. With respect to the formation enthalpy of the crystalline reference state (c.r.s.), we can determine the vitrification enthalpy for glassy state samples with the following scheme:



where c.r.s. denotes the crystalline reference system, i.e., the mechanical mixture of crystalline equilibrium phases corresponding to the glass composition.

Pure oxide mixtures with identical composition were prepared from pure α -alumina, silica glass, calcium oxide and magnesium oxide. Calcium oxide and magnesium oxide were prepared from calcium carbonate or magnesium hydroxide carbonate, respectively by decomposition at about 1300 K for 12 h in an alumina crucible in air. The oxide powders thus obtained were transferred in desiccators to a glove box in which an atmosphere from H_2O and CO_2 was maintained; the material was stored here in desiccators until use. Examination of the substances by X-ray diffraction employing Cu K_α radiation detected well-crystallized pure oxides. From the fine powders of the component oxides, pure oxide mixtures with compositions identical to the glass compositions were prepared in the glove box. The required amounts of the oxides were weighed out and mixed in an agate mixer mill (with three-dimensional motion for colloidal micro-grinding and homogeneous mixing) and pressed in the form of pellets. In order to protect the oxide mixtures from H_2O and CO_2 in the air, they were taken individually from the glove box to the calorimeter, using the sample holder described below. When this holder had been connected to the charging tube of the calorimeter by a ground glass joint, the sample was dropped from the sample holder into the calorimeter in order to start the experiment.

The partial molar mixing enthalpies of CaO ($\Delta H^{\text{mix}}_{\text{CaO}}$) were determined from the enthalpy difference between the directly measured enthalpy $\Delta H^1 (T_K - T_0)$ and calculated enthalpy $\Delta H^2 (T_K - T_0)$ using the heat capacity of CaO with the following scheme:



For the determination of partial molar mixing enthalpies of CaO ($\Delta H^{\text{mix}}_{\text{CaO}}$), CaO pellets with masses between 5 and 10 mg were dropped into the melts about 5 g at high temperature (T_K). The influence of CaO pellets on the composition of the melts is negligible.

CaO pellets were prepared from calcium carbonate by decomposition at about 1300 K for 12 h in air. The CaO pellets thus obtained were transferred in desiccators to a glove box; the material was stored here in desiccators until use. Examination of the substance by X-ray diffraction employing Cu K_{α} radiation detected only CaO oxide. In order to protect the calcium oxides from H_2O and CO_2 in the air, they were taken individually from the glove box to the calorimeter, using the sample holder like transferring of oxide mixtures. And then measurements were performed as stated above.

The main part of the sample holder, figure 3.17, consists of a glass tube enlarged spherically in the middle. The sample is introduced into this spherical part through a side arm, which is closed by a ground glass stopper. The spherical part is sealed above and below by O-rings mounted on a glass rod. The sample is released from the holder by lifting the glass rod.

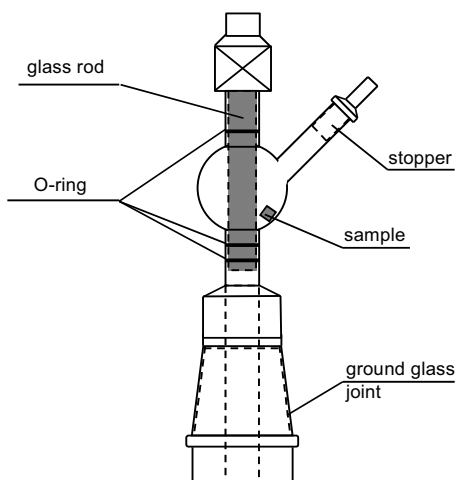


Fig. 3.17 Sample holder attached by means of a glass joint to the upper end of the charging tube.

In the calorimetric measurements performed in this study, a platinum crucible was located in the working crucible in order to protect the alumina-working crucible from attack by the molten glass. Before initiating an experiment, the platinum crucible was charged with about 5 g for each glass of the composition

in order to melt probes quickly at calorimeter temperature and to transfer heat flux easily to the detector. During the experiment, each glass and oxide mixture sample with masses between 10 and 15 mg was dropped into the calorimeter at high temperature. In alternating sequence with the samples, platinum spheres were dropped into the calorimeter for calibration. The enthalpy effects associated with the reactions occurring in the calorimeter are presented exemplarily in figure 3.18.

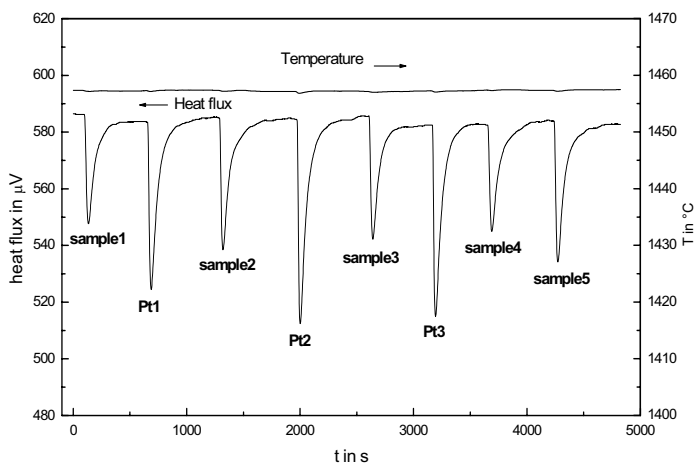


Fig. 3.18 The enthalpy effects associated with the reactions occurring in the calorimeter

4 Thermodynamic modeling

In this work two models are adopted to calculate thermodynamic properties in multi-component oxide melts. One is the constitutional model by Conradt [CON 1998] to calculate activities of CaO, vitrification enthalpies and melting enthalpies, another is a commercial software F*A*C*T [BAL 2002] to calculate activities of CaO.

4.1 Constitutional model

For the calculation of the thermodynamic properties it is important to note that the melt or glass of a multi-component system may be conceived as a nano scale mixture [CON 2000]. In the point of view of mixing thermodynamics, the nano scale mixture refers to the range where the concepts of heterogeneous and homogeneous mixtures overlap. There is ample experimental proof that the nano scale nature is reflected by many properties of the solid glass, even of the glass melt above T^m . The nano scale nature of species distribution does not imply that the glass itself is a heterogeneous system. As earlier predicted by theory [ADA 1965], many glass-forming systems are not homogeneous down to the molecular scale.

The Gibbs energy of a heterogeneous mixture of individual compounds k is presented by

$$G = \sum_k n_k \cdot G_k^0 + G^x \quad (4.1)$$

with an interfacial term

$$G^x = \sum_k n_k \cdot \sigma_k \cdot A_k \cdot M_k = \sum_k n_k \cdot \sigma_k \cdot \Phi \cdot V_k / L \quad (4.2)$$

where σ_k denotes the surface tension; A_k is the specific surface area, V_k the molar volume, Φ a geometrical factor, and L is a length parameter characterizing the average size of particles of compounds k . As a consequence, the surface term G^x can be neglected for macroscopical mixtures, but plays a significant role for very small sizes.

Due to the reasons explained above, thermodynamic potentials of constitutional compounds k are used to derive properties of multi-component system. These compounds are stoichiometric quantities with the same stoichiometry as the phases of the corresponding phase diagram. The composition itself is expressed by a set of stoichiometric components. The set of constitutional compounds is employed in this work for this purpose, offering a swift and easy approach to the thermodynamic potentials Z .

The thermodynamic potentials from the elements of a multi-component glass, Z_{glass} , is given by

$$Z_{\text{glass}} = Z_{\text{cryst}} + Z^{\text{vit}} \quad (4.3)$$

like for a one-component system. However, Z_{cryst} is given by

$$Z_{\text{cryst}} = \sum x_k \cdot Z^*_k \quad (4.4)$$

where x_k denotes the molar fraction of the constitutional equilibrium compound (or co-existing crystalline phase) k , and Z^*_k denotes the energies of the pure crystalline substances. When the term Z^{vit} is distributed to individual terms, then Z_{glass} may be expressed as

$$Z_{\text{glass}} = \sum X_k \cdot (Z^*_k + Z'_k) \quad (4.5)$$

Z'_k majorly accounts for the difference between the glassy and crystalline state of compound k . Since the glass is an apparently homogeneous phase, Z'_k should also comprise the effects of mixing. But an evaluation of experimental results suggests that this contribution of mixing effects to the thermodynamic potentials can be neglected. Examples are the heats of mixing in the ternary systems $\text{NaAlSi}_3\text{O}_8$ (ab) – $\text{CaAl}_2\text{Si}_2\text{O}_8$ (an) – $\text{CaMgSi}_2\text{O}_6$ (di) [NAV 1980] and $\text{NaAlSi}_3\text{O}_8$ (ab) – KAlSi_3O_8 (or) – Si_4O_8 (Q) [HER 1984]. According to Navrotsky [NAV 1980], the system ab – di shows positive heats of mixing, while ab – an and di – an show negative heats of mixing. Thus the ternary system includes a contour of zero heat of mixing. Hervig [HER 1984] showed that the system or –

Q has zero heats of mixing similar to that for ab – Q system, while ab – or system has negative heats of mixing symmetric about ab_{50} or 50_{50} .

Hence Z'_k may be expressed as

$$Z'_k \approx Z_k^{vit} \quad (4.6)$$

and

$$Z_{glass} = \sum X_k \cdot Z_{k,glass} \quad (4.7)$$

For the melt (above the melting temperature T^m),

$$Z_{melt} = \sum X_k \cdot Z_{k,melt} \quad (4.8)$$

The above thermodynamic presentation of multi-component glasses and glass melts in terms of the constitutional equilibrium compounds k of the glass forming system is used to calculate activities and energies of vitrification.

The activity calculation procedure is: Firstly, the constitutional compounds of the respective melt are identified by a unified norm calculation similar to the C.I.P.W. norm [PHI 1990] used in geology. Then, the activities of individual oxides are calculated by linear combinations of the Gibbs energies of formation of these compounds from the oxides. The procedure is based on a thorough evaluation of the phase relations in existing phase diagrams. The fact used is that n -component phase diagrams can be broken down into compositional sub-ranges with n corners, each corner representing a constitutional compound k . These are sub-triangles in ternaries, sub-tetrahedron in quaternaries, respectively. In this approach the oxides are counted among the k , (constitutional compounds) too. For each of the sub-ranges, the molar amounts n_j of oxides j are converted into molar amounts n_k of the corner compounds by the operation. The calculation of constitutional compounds is described in chapter 3.1.2 in detail.

$$n_j = (V_{kj}) \cdot n_k \rightarrow n_k = (A_{jk}) \cdot n_j \quad (4.9)$$

The matrix element V_{kj} is given by the number of moles of oxide j contained in one mol of compound k . A_{jk} is the element of the inverted matrix $(V_{kj})^{-1}$. The molar fractions $x_k = n_k / \sum n_k$ represent the concentration distribution spectrum of the k within the respective sub-range. Activities are calculated by equating the Gibbs energies in both component frames j and k :

The Gibbs energy is expressed

$$\Delta G = G_k^0 - \sum V_{kj} \cdot G_j^0 \quad (4.10)$$

from this equation an equilibrium constant is calculated as

$$\ln K_k = -\frac{1}{R \cdot T} \cdot \left[G_k^0 - \sum V_{kj} \cdot G_j^0 \right] \quad (4.11)$$

the equilibrium constant is also represented by

$$\ln K_k = \ln a_k - \sum V_{kj} \cdot \ln a_j \quad (4.12)$$

The combination of equations 4.11 and 4.12 results in

$$G_k^0 + RT \ln a_k = \sum V_{kj} \cdot \left[G_j^0 + RT \ln a_j \right] \quad (4.13)$$

yielding the following expression for the activity coefficient f_j of oxide j , :

$$\ln a_j = \sum_k A_{jk} \cdot \left[\frac{G_k^0}{R \cdot T} + \ln a_k \right] - \frac{G_j^0}{R \cdot T} \quad (4.14)$$

The G_j^0 , G_k^0 are standard Gibbs energies of the pure k , j , respectively, in the desired reference state.

As stated at the beginning of this chapter, the glassy and liquid state of a multi-component system is considered essentially as a nano scale mixture. It has been shown that due to the small contributions of mixing energies, the homogeneous silicate systems considered can be presented by the same formation, i.e., by weighted means of their constitutional components. Let us consider in the point of view of mixing thermodynamics that our mixture is a heterogeneous system. It means that the activity of constitutional compounds a_k in the equation 4.14 becomes one. Then this equation is represented as follows:

$$\ln a_j = \sum_k A_{jk} \cdot \left[\frac{G^0_k}{R \cdot T} \right] - \frac{G^0_j}{R \cdot T} \quad (4.15)$$

Here, $\ln a_j$ means the average of activities of oxide j in the heterogeneous mixture. In addition, let us consider that our mixture is a homogeneous system. The Gibbs energy of a homogeneous mixture of arbitrarily chosen components j is expressed by

$$G = \sum n_j \cdot G^0_j + G^{mix}_j \quad (4.16)$$

with a mixing term

$$G^{mix}_j = R \cdot T \sum n_j \cdot \ln a_j = H^{mix}_j - T \cdot S^{mix}_j \quad (4.17)$$

For a distinguished set of components $j = k$, H^{mix}_k approaches zero, as in the examples of Navrotsky [NAV 1980] and Hervig [HER 1984]. Additionally, S^{mix}_k becomes a merely statistical term. It is given by Boltzmann' relation

$$S^{mix}_k = -k \cdot \ln W = -k \cdot \sum_k N_k \cdot \ln x_k \quad (4.18)$$

Here N_k is the number of molecular units of k , $N = \sum N_k$ is the total number of units. The term $\ln x_k$ requires a statistical mixing on the atomic level (based on $6.023 \cdot 10^{23}$ units per mol). Upon slight clustering [CON 1997], however, the number N_k of units available for statistical mixing decreases. With a clustering of only 4 short-range order distances, N_k - and hence S^{mix}_k - is decreased by a factor of 4^3 . Thus G^{mix} , and hence $\ln x_k$, become obsolete, and equation 4.15 describes the oxide activities also in the homogeneous glass or melt.

In the absence of clustering, equation 4.17 is represented by

$$G^{mix}_k = -T \cdot S^{mix}_k = R \cdot T \sum n_k \cdot \ln x_k \quad (4.19)$$

leading to a presentation of G as

$$G = \sum n_k \cdot G_k^0 + R \cdot T \sum n_k \cdot \ln x_k \quad (4.20)$$

The combination of equations 4.13 and 4.20 results in

$$\ln a_j = \sum_k A_{jk} \cdot \left[\frac{G_k^0}{R \cdot T} + \ln x_k \right] - \frac{G_j^0}{R \cdot T} . \quad (4.21)$$

As a result, we obtain two equations, i.e., equation 4.15 and 4.21 to calculate oxide activities a_j . The former one is valid for clustered (highly associated) liquids and glasses, the latter one is valid for liquids and glasses statistically mixed on the atomic level. One may criticize this approach in that it does not offer an a priori approach to decide which of the two above options has to be chosen for an unknown system.

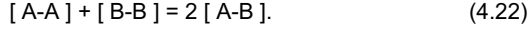
The constitutional model using equation 4.21 has a further weak point to calculate oxide activities at the edges of a constitutional range. At the edges of a constitutional range, at least one x_k becomes zero, the calculating for oxide activity is meaningless. This problem is bypassed by determining the values in the center of each constitutional range (i. e., at $x_k = 0.5$ in a binary system) and connecting the activity values obtained at these points by polygons. The strong point is that no adjustable parameters are used and that no complications occur for systems with a very large number of components.

4.2 Modified quasichemical model

The modified quasichemical model was developed by Pelton and Blander [BLA 1983, PEL 1986] to apply to ordered liquid solutions such as slags. This model, which is based on modifications of the quasichemical theory of Guggenheim [GUG 1935, FOW 1939], takes into account the concentration and temperature dependence of the solution properties of ordered systems and thus enhances the reliability of interpolations and extrapolations of data.

The quasichemical theory treats a binary system with components "A" and "B" in which "A" and "B" particles mix substitutionally on a quasi-lattice with a constant coordination number z . There are three types of nearest-neighbour pairs (namely, A-A, B-B, and A-B) with "pair bond energies" ε_{ij} . The total number of such pairs per mole of solution is $N^0 z / 2$ where N^0 is Avogadro's number.

Consider two A-B pairs are formed from an A-A and a B-B pair according to reaction 4.22



Then the enthalpy change for this process is $(2\varepsilon_{AB} - \varepsilon_{AA} - \varepsilon_{BB})$. Multiplying by $N^0 z/2$, one define a molar enthalpy change, ω :

$$\omega = \frac{N^0 z}{2} (2\varepsilon_{AB} - \varepsilon_{AA} - \varepsilon_{BB}). \quad (4.23)$$

One can also define a molar nonconfigurational entropy change, γ , associated with reaction (4.22) as:

$$\gamma = \frac{N^0 z}{2} (2\sigma_{AB} - \sigma_{AA} - \sigma_{BB}), \quad (4.24)$$

where σ_{ij} is the “nonconfigurational entropy of the pair bond”. Let n_A and n_B be the number of moles of “A” and “B” particles. For one mole of solution, $(n_A + n_B) = 1$. The mole fractions of A and B are defined as $X_A = n_A/(n_A + n_B) = 1 - X_B$. Let n_{AA} , n_{BB} , and n_{AB} be the number of moles of each type of pair in solution. The fraction of pairs, which are i-j pairs, is defined as:

$$X_{ij} = \frac{n_{ij}}{(n_{AA} + n_{BB} + n_{AB})}. \quad (4.25)$$

Each “A” particle is bonded to zn_A neighbours. Therefore, from the mass balance it follows that:

$$zn_A = 2n_{AA} + n_{AB}. \quad (4.26)$$

Similarly:

$$zn_B = 2n_{BB} + n_{AB}. \quad (4.27)$$

From equation 4.25 through 4.27, then:

$$2X_A = 2X_{AA} + X_{AB} \quad (4.28)$$

$$2X_B = 2X_{BB} + X_{AB}. \quad (4.29)$$

When components "A" and "B" are mixed, A-B pairs are formed at the expense of A-A and B-B pairs. In the model, the enthalpy of mixing, ΔH , is then given by summing the pair bond energies:

$$\Delta H = \frac{X_{AB}}{2} \omega. \quad (4.30)$$

The nonconfigurational entropy of mixing is expressed similarly:

$$\Delta S^{\text{nonconfig}} = \frac{X_{AB}}{2} \gamma. \quad (4.31)$$

To obtain an expression for the configurational entropy of mixing one must calculate the multiplicity of a solution containing n_{AA} , n_{BB} , and n_{AB} moles of A-A, B-B, and A-B pairs. This problem has not been solved in three dimensions. In the approximate solution proposed by Guggenheim [GUG 1935], the pairs are distributed randomly over the $N^0z/2$ positions to give a molar entropy of mixing of:

$$\Delta S = -\frac{Rz}{2} (X_{AA} \ln X_{AA} + X_{BB} \ln X_{BB} + X_{AB} \ln X_{AB}). \quad (4.32)$$

This, however, counts excessively the number of possible configurations. A correction factor is calculated from the fact that when the solution is completely random: $X_{AA} = X_A^2$, $X_{BB} = X_B^2$, $X_{AB} = 2X_A X_B$, and ΔS should equal $-R(X_A \ln X_A +$

$X_B \ln X_B$). Therefore, the approximate configurational entropy of mixing expression proposed by Guggenheim is:

$$\Delta S^{config} = -R(X_A \ln X_A + X_B \ln X_B) - \frac{Rz}{2} \left(X_{AA} \ln \frac{X_{AA}}{X_A^2} + X_{BB} \ln \frac{X_{BB}}{X_B^2} + X_{AB} \ln \frac{X_{AB}}{2X_A X_B} \right). \quad (4.33)$$

Hence, the total molar excess entropy (configurational plus nonconfigurational) of the solution is given from equations 4.31 and 4.33 as:

$$S^E = -\frac{Rz}{2} \left(X_{AA} \ln \frac{X_{AA}}{X_A^2} + X_{BB} \ln \frac{X_{BB}}{X_B^2} + X_{AB} \ln \frac{X_{AB}}{2X_A X_B} \right) + \left(\frac{X_{AB}}{2} \right) \gamma. \quad (4.34)$$

The equilibrium concentrations of the various pairs are given by minimizing the Gibbs energy at constant compositons:

$$\frac{d(\Delta H - T \Delta S)}{dX_{AB}} = 0. \quad (4.35)$$

This gives:

$$\frac{X_{AB}^2}{X_{AA} X_{BB}} = 4e^{-2(\omega - \gamma T) / zRT}. \quad (4.36)$$

Equation 4.36 resembles an equilibrium constant for reaction 4.22. It is for this reason that the model is called “quasichemical”. Substitution of equations 4.28 and 4.29 into equation 4.36 gives:

$$\frac{X_{AB}}{2} = \frac{2X_A X_B}{(1 + \xi)}, \quad (4.37)$$

where $\xi = [1 + 4X_A X_B (e^{2(\omega - \gamma T) / zRT} - 1)]^{1/2}$.

For a given value of $(\omega - \gamma T)$ at a given composition X_A , equation 4.37 gives X_{AB} and equations 4.28 and 4.29 then give X_{AA} and X_{BB} . Substitution into equations 4.30 and 4.34 then gives ΔH and S^E .

If $\omega = 0$ and $\gamma = 0$, then $\Delta H = 0$ and $S^E = 0$ and the solution is ideal. When ω and γ are small, $S^E \approx 0$ and $X_{AB} \approx 2X_A X_B$. From equation 4.30 then, $\Delta H \approx X_A X_B \omega$. That is, the solution is regular. The approach is nowadays commonly accepted. The parameters ω , γ , ξ are derived from an evaluation of existing thermodynamic data and phase diagrams and adjusted accordingly. The model thus heavily depends on adjustable parameters, which becomes increasingly complicated and numerically unstable as the number of components in a system increases. A change of a single data set for a compound may upset the entire system of parameters. The univocal strength of the system is the comprehensive presentation of all thermodynamic quantities of a system, comprising all phase transitions.

5 Results and discussion

5.1 Results of calculation and EMF measurement

5.1.1 Calculation of oxide activities in the melts

By using the constitutional model described in chapter 4.1, the activities of CaO are calculated in the temperature range from 1300 K to 1800 K. The results are plotted in figure 5.1 and listed in table 5.1.

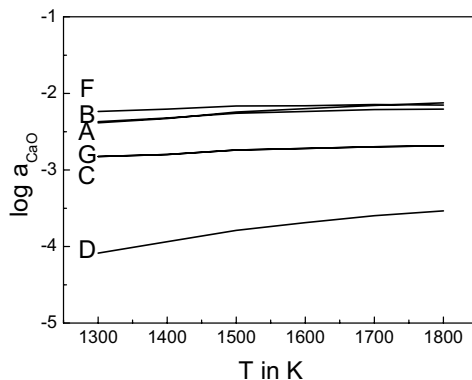


Fig. 5. 1 Calculated activities of CaO with temperature in six melts considered as a nano scale mixture using the constitutional model

For the calculation of oxide activity in the multicomponent systems using the constitutional model, we have to identify the correct set of k , i. e., the crystalline reference state for a given composition. The calculation method for crystalline reference state was explained in detail in chapter 3.1.2. The calculated crystalline reference states for six glassy samples are listed in table 5.2.

According to the equation 4.15, Gibbs energies of constitutional compounds and oxide are required to calculate oxide activities by the constitutional model. Gibbs energies of constitutional compounds and oxide, which are used for the calculation of oxide activities in this work, are listed in table 5.3

Tab. 5.1 Decadal logarithms of thermodynamic activities ($\log a$) of CaO and activity coefficient ($\log f$) in six glasses melt using the constitutional model

		$\log a_{\text{CaO}}$					
T in K	A	B	C	D	F	G	
1300	-2.369	-2.383	-2.825	-4.086	-2.236	-2.825	
1400	-2.321	-2.328	-2.798	-3.936	-2.206	-2.798	
1500	-2.261	-2.243	-2.741	-3.789	-2.165	-2.741	
1600	-2.236	-2.200	-2.719	-3.689	-2.161	-2.719	
1700	-2.211	-2.157	-2.698	-3.598	-2.146	-2.698	
1800	-2.205	-2.124	-2.684	-3.535	-2.153	-2.684	
		$\log f_{\text{CaO}}$					
T in K	A	B	C	D	F	G	
1300	-1.763	-1.910	-2.251	-3.215	-1.696	-2.264	
1400	-1.715	-1.855	-2.224	-3.065	-1.666	-2.237	
1500	-1.655	-1.770	-2.167	-2.918	-1.625	-2.180	
1600	-1.630	-1.727	-2.145	-2.818	-1.621	-2.158	
1700	-1.605	-1.684	-2.124	-2.727	-1.606	-2.137	
1800	-1.599	-1.651	-2.110	-2.664	-1.613	-2.123	

Tab. 5.2 Calculated crystalline reference states of six glassy samples given in wt. %

Samples Oxides	A	B	C	D	F	G
CAS ₂	42.02	45.84	34.38	46.66	40.79	39.02
CMS ₂	57.27	2.01	24.17	11.95	-	-
S	0.36	-	17.82	18.04	-	26.31
MS	0.35	-	-	23.35	-	-
C ₂ MS ₂	-	52.12	-	-	46.43	-
M ₂ S	-	0.04	-	-	12.1	-
CS	-	-	23.63	-	-	34.67
C ₂ AS	-	-	-	-	0.68	-

We also used commercial software F*A*C*T [BAL 2002] to calculate activities of CaO in the melts. By using the commercial software F*A*C*T, the activities of CaO are calculated in the temperature range from 1300 K to 1800 K. The results are plotted in figure 5.2 and listed in table 5.4.

Tab. 5.3 Gibbs energies of constitutional compounds and oxide. [CON 1999]

T in K k	- G_k^0 in kJ/mol					
	1300	1400	1500	1600	1700	1800
CAS ₂	4684.4	4753.0	4824.6	4898.6	4975.6	5055.1
CMS ₂	3557.7	3612.0	3669.4	3728.8	3790.3	3854.3
C ₂ MS ₂	4345.9	4414.5	4486.1	4560.6	4637.5	4717.0
M ₂ S	2409.1	2445.1	2482.4	2521.3	2561.4	2602.4
MS	1709.6	1735.9	1763.6	1792.0	1821.3	1851.8
C ₂ AS	4420.8	4489.9	4561.8	4636.7	4713.7	4793.2
CS	1816.7	1845.6	1875.7	1907.1	1939.7	1973.2
S	1017.5	1030.5	1044.7	1059.4	1074.9	1091.2
CaO	728.9	740.1	752.3	764.4	777.0	789.5

As shown in figure 5.2, F*A*C*T considers the samples as solid state with crystalline phases below the solidus temperature and as melts above the liquidus temperature. In a range between solidus and liquidus temperature the samples are considered as partially crystalline.

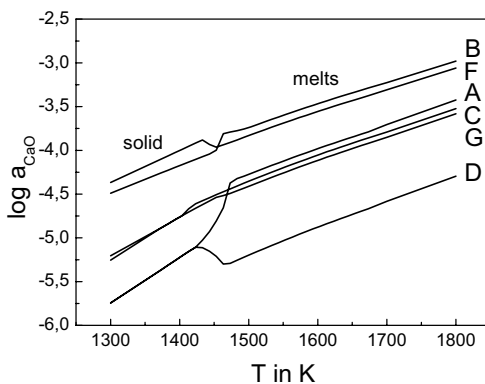


Fig. 5.2 Calculated activities of CaO with temperature in six melts using F*A*C*T

Tab. 5.4 Decadal logarithms of thermodynamic activities ($\log a$) of CaO and activity coefficient ($\log f$) in 6 glasses melt using $F^*A^*C^*T$

		$\log a_{CaO}$					
T in K	A	B	C	D	F	G	
1300	-5.783	-4.511	-5.255	-5.783	-4.396	-5.255	
1400	-5.224	-4.173	-4.762	-5.224	-4.000	-4.762	
1500	-4.275	-3.742	-4.353	-5.198	-3.831	-4.411	
1600	-3.981	-3.467	-4.054	-4.878	-3.556	-4.115	
1700	-3.722	-3.226	-3.790	-4.595	-3.314	-3.852	
1800	-3.492	-3.012	-3.557	-4.344	-3.099	-3.618	
		$\log f_{CaO}$					
T in K	A	B	C	D	F	G	
1300	-5.177	-4.038	-4.681	-4.912	-3.856	-4.693	
1400	-4.618	-3.700	-4.188	-4.353	-3.460	-4.200	
1500	-3.669	-3.269	-3.779	-4.327	-3.291	-3.849	
1600	-3.375	-2.994	-3.480	-4.007	-3.016	-3.553	
1700	-3.116	-2.753	-3.216	-3.724	-2.774	-3.290	
1800	-2.886	-2.539	-2.983	-3.473	-2.559	-3.056	

In the following chapter, we compare the calculated values with directly measured values by EMF method.

5.1.2 Experimental results

First of all, at the composition of $CaO \cdot 6Al_2O_3$ the EMF measurement was carried out at a temperature range from 1200 K to 1500 K using partially ion-exchanged calcium β^* -alumina solid electrolyte in order to determine the ionic transport number, t_{ion} , of the solid electrolyte. CaO was used as reference. The EMF vs. temperature plots of the following cell reaction is presented in figure 5.3.a and ionic transport number are determined by the equation 3.3 and given in figure 5.3.b.

Pt / Air / CaO(s), Pt / Ca β^* -alumina / CaO $\cdot 6Al_2O_3$ (s), Al_2O_3 (s), Pt / Air / Pt

$$E = - \frac{R \cdot T}{2 \cdot F} \cdot \int_{a_{CaO}^{right}}^{a_{CaO}^{left}} t_{Ca^{2+}} d \ln a_{CaO} \quad (3.3)$$

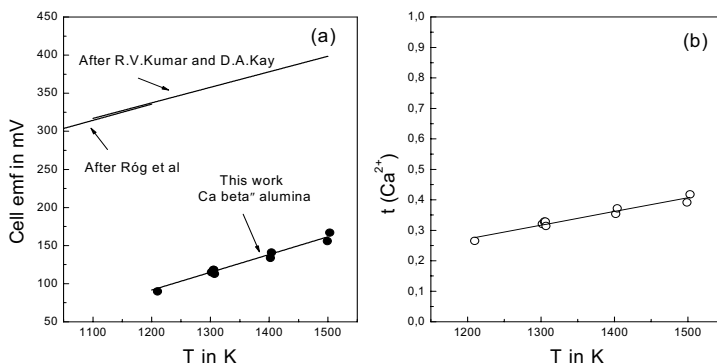


Fig. 5.3 (a) Variation of EMF with temperature for the cell using partially ion-exchanged calcium β'' -alumina
 (b) Variation of ionic transport number of CaO, $t_{\text{Ca}^{2+}}$, with temperature for the ion-exchanged calcium β'' -alumina

The EMF measured by partially ion-exchanged calcium β'' -alumina are compared with the literature values determined by the solid-state synthesized Ca β'' -alumina from Kumar and Kay [KUM 1985]. The slope (0.233 mV/K) of the EMF versus temperature function is similar to that (0.204 mV/K) obtained by Kumar and Kay [KUM 1985], in the temperature range from 1100K to 1500K. The results are also compared with the literature values measured by the completely ion-exchanged calcium β'' -alumina by Róg [ROG 1993]. Also, in this case, the slope of EMF increase is similar to that from Róg (0.213 mV/K) in the temperature range from 1000K to 1200K. But the EMF values obtained from this experiment differ by less than a half of those from the literature. This difference could be caused by the un-exchanged sodium (20.2%) and silver (7.3%) ions in the partially ion-exchanged calcium β'' -alumina listed in table 5.5. This assumption is based upon Wagner's line of reasoning [WAG 1933, WAG 1966]. A brief description is given below to consider an ionic transport number in the partially ion-exchanged calcium β'' -alumina.

Tab. 5.5 Degree of ion exchange in sodium β'' -alumina; number of measurements (n)

	start	after 1st exchange	after 2nd exchange
Na ₂ O	0.175 mol	0.035 mol	0.035 mol
Ag ₂ O	0.000 mol	0.140 mol	0.014 mol
CaO	0.000 mol	0.000 mol	0.126 mol
degree of ion exchange corresponding to step		79.8 %	90.8 %
degree of ion exchange corresponding to start		79.8 %	72.0 %
mass in g	100	123.7 ± 0.1 (27)	101.2 ± 0.7 (15)

Consider an electrochemical cell made up of a solid compound, MO, in which oxygen ions, O²⁻, excess electrons, e', and electron holes, h', are mobile, with oxygen chemical potentials μ'_{O_2} and μ''_{O_2} at the left-hand and right-hand electrode-electrolyte interfaces, respectively, as shown below:



The partial current density, I_i , of a mobile species, i , at any location within the electrolyte may be written as

$$I_i = \frac{-\sigma_i}{n_i F} \frac{d\mu_i}{dx}, \quad (5.1)$$

where σ_i is the partial conductivity of species i , n_i is the valence of i , F is the Faraday constant, x is the distance coordinate, and μ_i is the electrochemical potential of species i defined by

$$\mu_i = \mu_i^0 + n_i FE. \quad (5.2)$$

Here μ_i^0 is the chemical potential of i and E is the local electrostatic potential. In view of equations 5.1 and 5.2, the sum of the current densities of the oxygen ions, excess electrons, and electron holes in MO may be written as

$$I_{O^{2-}} + I_{h'} + I_{e'} = \frac{-dE}{dx} (\sigma_{O^{2-}} + \sigma_{h'} + \sigma_{e'}) + \frac{\sigma_{O^{2-}}}{2F} \frac{d\mu_{O^{2-}}}{dx} + \frac{\sigma_{e'}}{F} \frac{d\mu_{e'}}{dx} - \frac{\sigma_{h'}}{F} \frac{d\mu_{h'}}{dx}. \quad (5.3)$$

In thermodynamic measurements, one is interested in the open-circuit condition, which may be defined as the limiting case where the sum $I_{O_2} + I_{h'} + I_{e'}$ tends to zero. Thus at open circuit, from equation 5.3,

$$dE = \frac{t_{O_2}}{2F} d\mu_{O_2} + \frac{t_{e'}}{F} d\mu_{e'} - \frac{t_{h'}}{F} d\mu_{h'} \quad (5.4)$$

where t_{O_2} , $t_{h'}$, and $t_{e'}$ are the transference numbers of oxygen ions, electron holes, and excess electrons, respectively, and are given by the ratios of the respective partial conductivities to the total conductivity, $\sigma_{O_2} + \sigma_{h'} + \sigma_{e'}$.

The following equilibria may be assumed at any location in MO:

$$1/2 O_2 + 2e' = O^{-2}, \quad (5.5)$$

$$h' + e' = \text{zero}. \quad (5.6)$$

From equations 5.5 and 5.6,

$$d\mu_{O_2} - 2d\mu_{e'} = 1/2 d\mu_{O_2}, \quad (5.7a)$$

$$d\mu_{h'} = -d\mu_{e'}. \quad (5.7b)$$

Equations 5.4 through 5.7b, with the further condition that $t_{O_2} + t_{h'} + t_{e'} = 1$, give

$$dE = \frac{t_{O_2}}{4F} d\mu_{O_2} + \frac{d\mu_{e'}}{F}. \quad (5.8)$$

Integrating from $x = 0$ to $x = L$, yields

$$\varphi'' - \varphi' = \frac{1}{4} \int_{\mu'_0}^{\mu''_0} t_{O_2} d\mu_{O_2} + \frac{1}{F} (\mu''_{e'} - \mu'_{e'}). \quad (5.9)$$

Since $\varphi'' - \varphi'$ equals the open-circuit voltage ($E_{O.C.}$) and $\mu'_{e'} = \mu^{Pt}_{e'} = \mu''_{e'}$, one has

$$E_{O.C.} = \frac{1}{4F} \int_{\mu'_{O_2}}^{\mu''_{O_2}} t_{O_2} d\mu_{O_2}. \quad (5.10)$$

The general form of equation 5.10 for oxide is

$$E_{O.C.} = \frac{1}{zF} \int_{\mu'_{oxide}}^{\mu''_{oxide}} t_{ion} d\mu_{oxide}. \quad (5.11)$$

Equation 5.11 forms the basis for thermodynamic measurements using solid electrolytes. According to equation 5.10, the measured open-circuit voltage, $E_{O.C.}$ (i.e. EMF) is a simple function of the oxygen chemical potentials at the electrolyte boundaries when $t_{ion} \geq 0.99$. When t_{ion} is less than 0.99, there is electronic conduction in the electrolyte and there may be a problem in maintaining desired chemical potentials at the electrode-electrolyte interfaces.

This concept of the ionic transport number described above was adopted to explain the difference between the measured EMF using partially ion-exchanged calcium β'' -alumina and the literature values measured by complete ion-exchanged calcium β'' -alumina. As shown in table 5.5, the ratio of sodium ions remaining in calcium β'' -alumina is 20.2%, and that of silver ions is 7.3%. It means that there are three different ionic transport numbers in the partially ion-exchanged calcium β'' -alumina, i.e., t_{Na^+} , $t_{Ag^{2+}}$ and $t_{Ca^{2+}}$. It is also thought that the ionic transport number of CaO ($t_{Ca^{2+}}$) is less than one because of the remaining sodium and silver ions in the solid electrolyte. According to equation 5.11, the measured EMF should be less than desired EMF when $t_{Ca^{2+}} < 0.99$. As compared with the literature values, the ionic transport number of CaO ($t_{Ca^{2+}}$) in the partially ion-exchanged calcium β'' -alumina was determined in temperature range 1200 K to 1500 K, it is given in figure 5.3 b on page 70.

On account of the ionic transport number of CaO ($t_{Ca^{2+}}$), which is less than 0.99, in the partially ion-exchanged calcium β'' -alumina, calcium magnetoplumbite solid electrolyte was used to measure EMF in this investigation. Calcium magnetoplumbite was confirmed to be CaO electrolyte by Fray [FRA 1993]. We measured also EMF of the following cell reaction using calcium magnetoplumbite as the electrolyte.

Pt / Air / CaO(s), Pt / Ca magnetoplumbite / CaO · 6Al₂O₃(s), Al₂O₃(s), Pt / Air / Pt

The difference between the measured EMF value using calcium magnetoplumbite synthesized in this work and the value from Kumar and Kay [KUM 1985] dose not exceed 20 mV for the above cell reaction at temperature

1508 K, i.e. it is not greater than a few percent of the measured EMF. From the comparison of both measured EMF values it could be supposed that the calcium magnetoplumbite has the ionic transport number of CaO $t_{\text{Ca}^{2+}} \approx 1$.

EMF measurement using calcium magnetoplumbite was carried out to determine activities of CaO in the liquid range of our glass forming compositions. In the measurement, two factors limited the temperature range. The lower temperature was limited owing to the liquidus temperature of the samples. And the upper temperature was limited owing to an increasingly aggressive attack of the melts on the electrolyte. Therefore the EMF measurement was performed in the temperature range from 1473 K to 1573 K for 5 h. In order to determine the activities of CaO in our reference melt (composition G), EMF experiment of the following cell reaction was performed first:



We tried to use pure CaO as reference electrolyte, but we could not determine activities of CaO in the reference melt G in this measurement. According to Tanabe [TAN 1996], the EMF between solid electrodes stabilized after reaching the desired temperature in approximately 10 h at 1572 K. This means that it takes a long time to stabilize the EMF in the case of solid electrode in spite of the high temperature. As described above, the EMF measurement in this investigation was performed for 5 h owing to the two limiting factors. A chemical reaction at the sample-electrolyte interface can result in a compositional change in the sample. In addition the sample-electrolyte reaction can also result in a solid reaction product, which forms a layer between the sample and the electrolyte, then the EMF is no longer given by equation 3.3. In the above measurement using CaO powder and sample G with the eutectic temperature 1443 K, the EMF did not stabilize within 10 h at temperature 1518 K.

The EMF measurements were carried out continuously between sample G and other samples. Figure 5.4 shows the EMF measurements between sample G and sample B with respect to temperature and time. As the liquidus temperature of sample B is 1523 K, measurements were performed in the temperature range

from 1530 K to 1560 K. As shown in figure 5.4, the EMF stabilized after reaching the desired temperature in approximately 1 hour. But we found also a variation of EMF as function of a measuring time on all occasions. It may be caused by the chemical reaction between the melts and the electrolyte, which would lead to a change of the composition at the electrode-electrolyte interface or would form a layer between the electrode and the electrolyte.

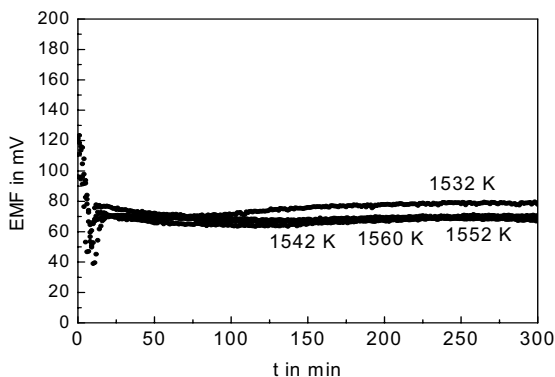


Fig. 5.4 EMF measurements between sample G and sample B with respect to temperature and time

Therefore we determined the EMF at the beginning of stabilization. With the aid of the measured EMF, activities of CaO in the melts were obtained using equation 3.4. But as explained above, unfortunately activities of CaO in the sample G could not be obtained. Hence for the determination of CaO activities in other samples, we used the calculated activities of CaO in sample G as reference from the constitutional model and $F^*A^*C^*T$, respectively. Table 5.6 shows the obtained activities of CaO in the five samples by the following cell reactions,



In table 5.6, we showed the measured CaO activities from three different standpoints. $\log^1 a_{\text{CaO}}$ in sample G is the CaO activities, which are calculated

using the constitutional model. On the other hand $\log^2 a_{\text{CaO}}$ and $\log^3 a_{\text{CaO}}$ in sample G are the CaO activities, which are calculated using $F^*A^*C^*T$. The difference between activities $\log^2 a_{\text{CaO}}$ and $\log^3 a_{\text{CaO}}$ is caused by the reference state of CaO. $\log^2 a_{\text{CaO}}$ is, as directly obtained by $F^*A^*C^*T$, related to the liquid state CaO and $\log^3 a_{\text{CaO}}$ is related to the solid state CaO as obtained by an additional calculation employing fusion data of CaO.

Tab. 5.6 Results of the CaO activities determined by the EMF measurements. The reference CaO activities in sample G are calculated using the constitutional model ($\log^1 a_{\text{CaO}}$) and $F^*A^*C^*T$ ($\log^2 a_{\text{CaO}}$, $\log^3 a_{\text{CaO}}$); $\log^1 a_{\text{CaO}}$ and $\log^3 a_{\text{CaO}}$ are solid CaO as reference, $\log^2 a_{\text{CaO}}$ is liquid CaO as reference.

Sample A				Sample B			
T in K	$\log^1 a_{\text{CaO}}$	$\log^2 a_{\text{CaO}}$	$\log^3 a_{\text{CaO}}$	T in K	$\log^1 a_{\text{CaO}}$	$\log^2 a_{\text{CaO}}$	$\log^3 a_{\text{CaO}}$
1541	-2.320	-3.871	-2.638	1532	-2.300	-3.862	-2.627
1550	-2.262	-3.801	-2.571	1542	-2.276	-3.868	-2.593
1560	-2.321	-3.864	-2.620	1552	-2.249	-3.815	-2.556
				1560	-2.260	-3.806	-2.559
Sample C				Sample D			
T in K	$\log^1 a_{\text{CaO}}$	$\log^2 a_{\text{CaO}}$	$\log^3 a_{\text{CaO}}$	T in K	$\log^1 a_{\text{CaO}}$	$\log^2 a_{\text{CaO}}$	$\log^3 a_{\text{CaO}}$
1502	-2.546	-4.213	-2.904	1529	-3.081	-4.622	-3.411
1503	-2.566	-4.237	-2.923	1541	-3.077	-4.610	-3.395
1517	-2.591	-4.202	-2.934	1570	-3.063	-4.512	-3.352
1533	-2.546	-4.142	-2.872				
1549	-2.502	-4.070	-2.813				
Sample F				Sample G (calc. values)			
T in K	$\log^1 a_{\text{CaO}}$	$\log^2 a_{\text{CaO}}$	$\log^3 a_{\text{CaO}}$	T in K	$\log^1 a_{\text{CaO}}$	$\log^2 a_{\text{CaO}}$	$\log^3 a_{\text{CaO}}$
1508	-2.091	-3.761	-2.443	1500	-2.741	-4.411	-3.101
1523	-2.187	-3.801	-2.523	1520	-2.737	-4.350	-3.076
1528	-2.187	-3.801	-2.519	1540	-2.732	-4.289	-3.051
1536	-2.129	-3.700	-2.453	1560	-2.728	-4.230	-3.027
1550	-2.093	-3.625	-2.402	1580	-2.723	-4.171	-3.002

For the comparison of the calculated activities from two models (constitutional model and $F^*A^*C^*T$), it is very important to note that the calculated activities using the constitutional model are related to the solid state CaO. On the contrary the calculated activities using the $F^*A^*C^*T$ are related to the liquid state CaO. Therefore $\log^3 a_{\text{CaO}}$ is converted from $\log^2 a_{\text{CaO}}$ using a thermodynamic data of CaO.

As given in table 5.6, the comparison of calculated CaO activities in sample G shows that the activities related to the solid state by $F^*A^*C^*T$ are in the similar degree of those by the constitutional model.

As mentioned in the preceding chapter, we compared the calculated values by two calculation procedures with directly measured values by EMF method. In figure 5.5 and 5.6 the experimental activities of CaO in table 5.6 were compared with the calculated activities by the constitutional model and $F^*A^*C^*T$, respectively. There are two concepts in the constitutional model to calculate oxide activities a_j (see chapter 4.1); one is for the nano scale mixture and another is for the statistically mixed system on the atomic level. We considered also that the glass is a homogeneous system on an atomic scale. In figure 5.5 we presented two different CaO activities calculated by means of equation 4.15 and 4.21.

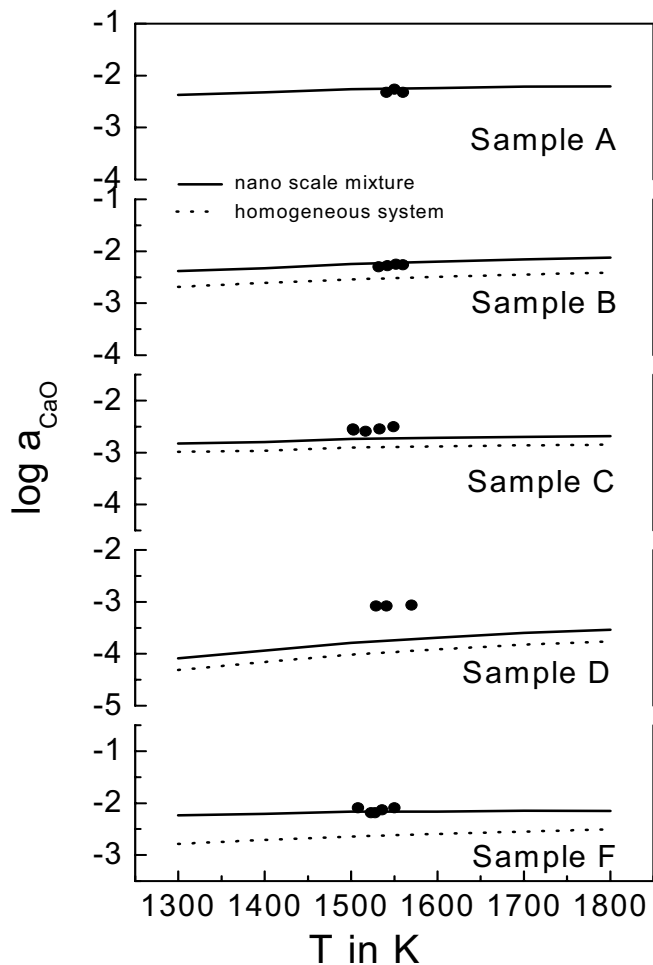


Fig. 5.5 Comparison of CaO activities between the calculated values by the constitutional model and the measured values by EMF method. Reference state is solid CaO.

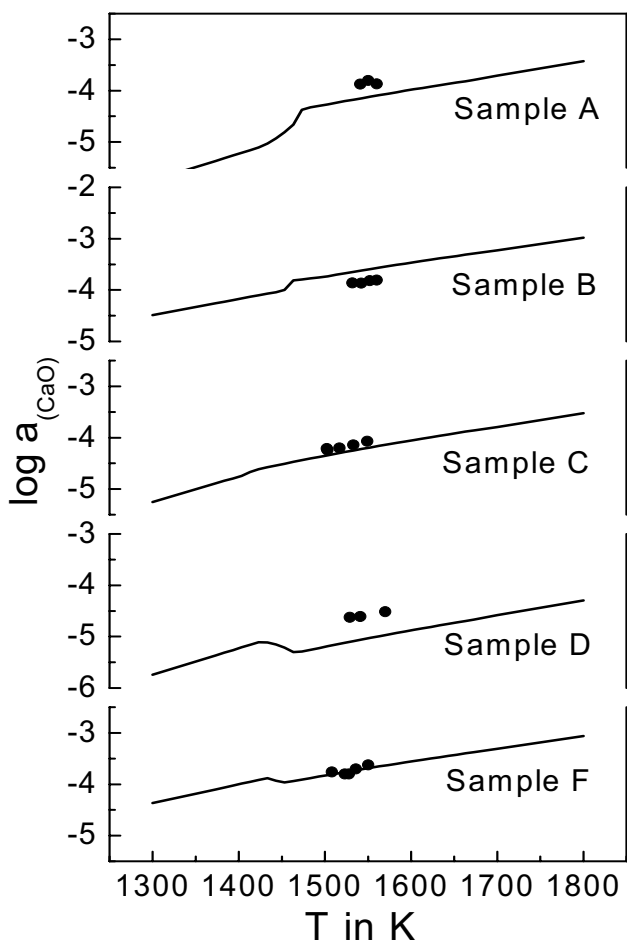


Fig. 5.6 Comparison of CaO activities between the calculated values by F*A*C*T and the measured values by EMF method. Reference state is liquid CaO

In figure 5.5 and 5.6 we show that the calculated activities by the constitutional model and F*A*C*T agree with the experimental values. Except for sample D, the calculated values are within ± 0.2 from the measured values as decadal

logarithms. The measured CaO activities in sample D differ from the calculated values about 0.5 ~ 0.7 degree in decadal logarithms as compared to both models. This fact could be assumed in the point of view of crystalline phases in sample D. As shown in chapter 3.1.2, the constitutional compounds of sample D are anorthite (CaSi_2), diopside (CaMgSi_2), cristobalite (S) and enstatite (MS). Of interest for the CaO activity calculation in sample D is the equilibrium phase of enstatite, because enstatite is the unique component detected in sample D among six samples. There are four condensed phases which occur at equilibrium; clinoenstatite (< 903 K), protoenstatite (<1258 K), orthoenstatite (<1850 K) and liquid enstatite [KNA 1991]. The difference between experimental and calculated values requires an intensive consideration in aspects of the thermochemical properties of constitutional compounds.

As previously stated, we could not determine the activity of CaO in the reference sample G owing to a few reasons described above. But we confirm from the comparison between experimental and calculated values that the electromotive force (EMF) technique is the useful method for the determination of oxide activity in silicate solutions.

5.2 Results of calorimetric measurement and calculation

5.2.1 Calculation of H^{vit} and $\Delta H_{\text{CaO}}^{\text{mix}}$

The calculation procedure for the vitrification enthalpy and melting enthalpy is based on the constitutional model explained at chapter 4.1. As previously stated, the application of thermodynamics has often been limited by the lack of reliable thermochemical data in multicomponent oxide systems. Data for oxide compounds in the liquid and glassy state are rare, and often extremely divergent. The data set for $\text{CaO}\cdot\text{Al}_2\text{O}_3\cdot 2\text{SiO}_2$ (anorthite) is depicted as an example. The melting enthalpy reported deviate from 81 kJ/mol [ROB 1978] to 166.9 kJ/mol [KNA 1991]. The vitrification enthalpy for anorthite deviate from 71.8 kJ/mol [KRA 1953] to 103 kJ/mol [FER 1971]. The literature data for anorthite is listed in table 5.7 and data for other oxide compounds are listed in Appendix.

Tab 5.7 Compilation of literature data for anorthite; melting enthalpy H^m , vitrification enthalpy H^{vit} at 298 K, melting temperature T^m , glass transition temperature T_g ; data based on diverse literatures.

H^m [kJ/mol]	H^{vit} [kJ/mol]	T_g [K]	T^m [K]	Reference
136	77.8		1830	[WEI 1980]
132.7	78.2		1830	[YOD 1976]
166.9	103		1830	[FER 1971]
	71.8			[KRA 1953]
133		1160	1830	[RIC 1984]
146	103	1113	1826	[CON 1999]
166.9			1826	[KNA 1991]
81			1830	[ROB 1978]
123			1823	[BAB 1985]
		1120		[SER 1995]
		1109		[STE 1995]

As shown in table 5.7, not only the melting enthalpies but also the vitrification enthalpies of anorthite reported are extremely divergent from different authors. It is true that the calculation procedure of thermodynamic models plays an important role in prediction and interpretation of thermochemical properties. And besides it is also very important for the calculation of the thermodynamic properties to select reliable thermochemical data in spite of a difficulty to find best available data sets. Using data set in appendix, the melting enthalpies and vitrification enthalpies of six samples were calculated with equation 4.7 and listed in table 5.8.

$$Z_{glass} = \sum X_k \cdot Z_{k,glass} \quad (4.7)$$

Tab. 5.8 Melting enthalpies H^m at T_{liq} and vitrification enthalpies H^{vit} of six samples calculated using equation 4.7

	A	B	C	D	F	G
H^m [kJ/mol]	124.3	146.0	61.5	57.3	123.6	50.7
H^{vit} [kJ/mol]	81.4	93.3	37.2	39.3	86.9	26.1

The partial molar mixing enthalpies of CaO, ΔH_{CaO}^{mix} , were calculated with the Gibbs-Helmholtz equation 2.22 from the activities of CaO calculated by the constitutional model or $F^*A^*C^*T$. It is needless to say that the accuracy of the partial molar mixing enthalpies of CaO obtained by this way is lower than that of

the direct measurements. As activities used for the calculation of the partial molar mixing enthalpies are derivative properties, the accuracy of partial molar mixing enthalpies is much poorer than that of calculated activities. The availability of direct, experimental partial molar mixing enthalpies is thus a real need.

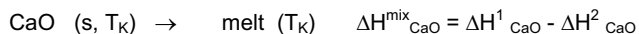
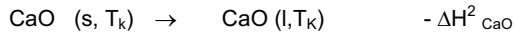
$$\Delta H^{\text{mix}}_j = -T^2 \left[\frac{\partial(\mu_j/T - \mu^0_j/T)}{\partial T} \right] = -RT^2 \left(\frac{\partial \ln a_j}{\partial T} \right) \quad (2.22)$$

By differentiating equation 2.22 with activities of CaO obtained by the constitutional model or F*A*C*T, partial molar mixing enthalpies were calculated and listed in table 5.9.

Tab 5.9 Partial molar mixing enthalpies of CaO, $\Delta H^{\text{mix}}_{\text{CaO}}$, calculated with Gibbs-Helmholtz equation from the activities of CaO calculated by the constitutional model and F*A*C*T

$\Delta H^{\text{mix}}_{\text{CaO}}$ [kJ/mol] from the constitutional model						
T in K	A	B	C	D	F	G
1500	-48.6	-24.3	-13.5	-48.6	-24.2	-13.1
1600	-47.2	-24.1	-11.6	-47.1	-24.1	-11.5
1700	-44.1	-23.2	-8.7	-44.0	-23.5	-9.1
1800	-39.2	-21.6	-4.9	-39.0	-22.1	-6.0
$\Delta H^{\text{mix}}_{\text{CaO}}$ [kJ/mol] from F*A*C*T						
T in K	A	B	C	D	F	G
1500	-53.2	-44.4	-55.4	-64.8	-44.7	-54.5
1600	-55.8	-46.6	-58.0	-67.9	-47.0	-57.4
1700	-55.5	-46.2	-57.8	-64.6	-46.6	-57.5
1800	-52.0	-42.6	-54.3	-67.2	-43.1	-54.4

For the calculation of partial molar mixing enthalpies by F*A*C*T, we must consider the reference state of CaO of F*A*C*T. As the commercial software F*A*C*T regards the reference state as liquid state, the melting enthalpy of CaO has to be summed with the following scheme:



where l, s denote liquid and solid state, respectively; according to $F^*A^*C^*T$, $\Delta H_{CaO}^2 = 79.5$ kJ/mol.

According to equation 2.22, the partial molar mixing enthalpy is a function of temperature, T , and a slope of nature logarithms of oxide activity, $\partial \ln a_j / \partial T$. As shown in figure 5.1 and 5.2, the slope of activities, as function of temperature T , obtained by the constitutional model is less than that obtained by $F^*A^*C^*T$. The difference of partial molar mixing enthalpy between both models can be calculated from the results of calculated activities. In the following chapter, we compare the partial molar mixing enthalpies calculated with direct measured values by drop calorimeter.

5.2.2 Experimental results of calorimetric measurement

We measured thermochemical properties in glassy state samples (i. e., glass transition temperature, c_p jump at T_g , vitrification enthalpy and partial molar mixing enthalpy) by calorimetric measurement.

The glass transition temperature T_g and the jump of the heat capacity Δc_p at T_g were measured by DSC as described in chapter 3.3. Thermal analysis curve of sample A was shown in figure 5.7 as an example and the measured values for all samples were listed in table 5.10.

As shown in figure 2.2, it is true that actual state of a solid glass depends not only on temperature, pressure, and chemical composition, but also on its history of vitrification. On account of this reason, all glassy samples were annealed at 800 °C for 4 h after completion of the melting process and cooled at 3 K/min to room temperature.

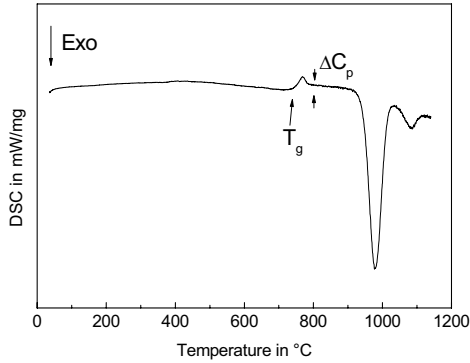


Fig. 5.7 Thermal analysis curve of sample A by DSC for the determination of T_g and ΔC_p at T_g

Tab 5.10 Glass transition temperatures and the jump of the heat capacity ΔC_p at T_g measured by DSC. T_{liq} is the melting temperature from phase diagram (A, B, G) or calculated (C, D, F)

	A	B	C	D	F	G
T_g in °C	742	750	748	764	739	788
ΔC_p in J/(g·K)	0.25	0.51	0.32	0.40	0.43	0.41
T_{liq} in °C	1274	1234	1138	1150	1163	1170

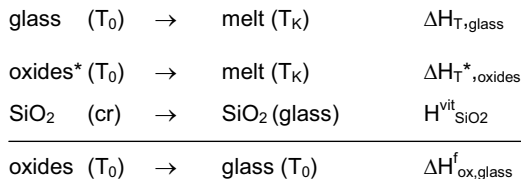
We show in table 5.10 that a proportion of T_g/T_{liq} agrees well with the following “rule of thumb” $T_g/T_{liq} = 2/3$.

The vitrification enthalpy was measured by the isothermal drop calorimeter as described in chapter 3.4. The measurements for the vitrification enthalpy were carried out in the temperature range from room temperature T_0 (295 K) to the calorimetric temperature T_K (1732 K). Enthalpy data were determined from the enthalpy difference $\Delta H (T_K - T_0)$ between room temperature and calorimeter temperature T_K . The measured values were listed in table 5.11.

Tab 5.11 Enthalpy increment $\Delta H_{T,\text{glass}}$, $\Delta H_{T^*,\text{Oxides}}$ measured by dropping glass samples and oxide mixtures (incl. The amount of SiO_2 as silica glass) into the calorimeter from room temperature ($T_0 = 295 \text{ K}$) to the calorimetric temperature ($T_K = 1732 \text{ K}$). $H_{\text{SiO}_2}^{\text{vit}} = 6.9 \text{ kJ/mol}$, after [CHA 1985]

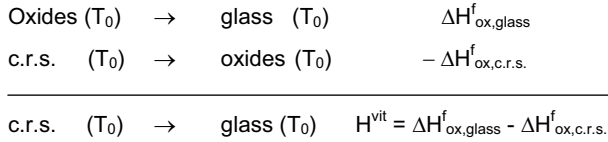
	$\Delta H_{T,\text{glass}}, \Delta H_{T^*,\text{Oxides}} \text{ [J/g]}$ number of measurements(n)	$n \cdot H_{\text{SiO}_2}^{\text{vit}}$ [J/g]	$\Delta H_{\text{ox,glass}}^f$ [J/g]
Glass A	1829.9 ± 40 (13)		-271.8
Oxide A	1500.1 ± 36 (8)	58.0	
Glass B	1795.6 ± 49 (7)		-194.1
Oxide B	1551.1 ± 34 (10)	50.4	
Glass C	1736.1 ± 48 (14)		-26.3
Oxide C	1642.8 ± 42 (18)	67.0	
Glass D	1809.9 ± 69 (14)		-48.0
Oxide D	1694.4 ± 50 (15)	67.5	
Glass F	2094.8 ± 57 (16)		-146.6
Oxide F	1898.4 ± 65 (13)	49.8	
Glass G	1749.7 ± 45 (13)		-165.9
Oxide G	1513.6 ± 38 (12)	70.2	

The formation enthalpy of glass from the oxides $\Delta H_{\text{ox,glass}}^f$ can be derived from the directly measured enthalpy difference with the following scheme:



As silica glass was used as pure silicon oxide at the measurement of oxide mixtures owing to a difficulty of dissolving the silicon oxide in the melt, an amount of vitrification enthalpy of silicon oxide, $H_{\text{SiO}_2}^{\text{vit}}$, must be summed to derive the formation enthalpy of glass from the oxides $\Delta H_{\text{ox,glass}}^f$.

With respect to the formation enthalpy of the crystalline reference state (c.r.s), we can obtain the vitrification enthalpy for glassy state samples with the following scheme:



where $\Delta H_{\text{ox,c.r.s.}}^{\text{f}}$ is the formation enthalpy of the crystalline reference state from the oxides. By using equation 4.7, the formation enthalpies of the crystalline reference states for six glassy samples were calculated and the vitrification enthalpy was also obtained from the difference of both values. In table 5.12 we showed the measured formation enthalpy of glass from the oxides $\Delta H_{\text{ox,glass}}^{\text{f}}$, the calculated formation enthalpy of the crystalline reference state $\Delta H_{\text{ox,c.r.s.}}^{\text{f}}$ and the vitrification enthalpy derived.

Tab 5.12 Vitrification enthalpy of six glassy samples derived from experimental and calculated values. $\Delta H_{\text{ox,glass}}^{\text{f}}$, measured by isothermal drop calorimeter and $\Delta H_{\text{ox,c.r.s.}}^{\text{f}}$, calculated using formation enthalpy of compounds at 298 K

	$\Delta H_{\text{ox,glass}}^{\text{f}}$ [J/g] measured	$\Delta H_{\text{ox,c.r.s.}}^{\text{f}}$ [J/g] calculated	H^{vit} [J/g]
Sample A	-271.8	-572.1	300.3
Sample B	-194.1	-547.7	353.6
Sample C	-26.3	-476.1	449.8
Sample D	-48.0	-352.9	304.9
Sample F	-146.6	-527.5	380.9
Sample G	-165.9	-402.7	236.8

The vitrification enthalpies and melting enthalpies for six glassy samples were calculated in the preceding chapter by the constitutional model. As stated in chapter 2.2.2, melting enthalpies can be calculated also with H^{vit} , ΔC_p , T_g and T_{liq} . We determined melting enthalpies using equation 2.28 with the experimental measured values: H^{vit} from the drop calorimeter measurements and ΔC_p , T_g from the DSC measurements. In table 5.13 we compared the values derived from the calorimetric measurements to the calculated values by the constitutional model and by equation 2.28.

$$H^{\text{fus}} - H^{\text{vit}} = \Delta C_p \cdot (T_{\text{liq}} - T_g) \quad (2.28)$$

Tab 5.13 Comparison of vitrification enthalpies between the measured and the calculated values.

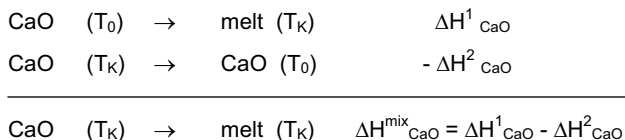
	H ^{vit} [J/g] measured by drop calorimeter	H ^{vit} [J/g] calculated by constitutional model	H ^m [J/g] calculated by constitutional model	H ^m [J/g] determined by eq. 2.25
Sample A	300.3	346.0	528.3	433.2
Sample B	353.6	340.9	533.7	608.4
Sample C	449.8	273.5	452.0	574.7
Sample D	304.9	297.1	432.7	475.4
Sample F	380.9	352.4	501.0	563.3
Sample G	236.8	229.1	444.5	393.6

After comparing of both values, we confirm that the vitrification enthalpies measured agree well with those calculated by the constitutional model, except for sample C.

According to Conradt [CON 1995, CON 1999], experimental data for H^{vit} of silicate systems suggests $H^{vit} \approx 0.6 H^m$. By surveying experimental data for H^{vit} and H^m (see appendix) of silicate systems, we confirm that the vitrification enthalpies can be estimated from the melting enthalpies. We showed also calculated melting enthalpies of six glassy samples by the constitutional model and equation 2.28 in table 5.14. These values suggest $H^{vit} = (0.6 \pm 0.09) \cdot H^m$, which is in good agreement with the above estimate, except for sample C.

But it goes without saying that there are obscurities at the comparing of values. As mentioned above, it is very important for the calculation of the thermodynamic properties to select reliable thermochemical data and to use available calculation procedure. It means that the thermodynamic properties may be changed depending on thermochemical data and on calculation procedure.

We also measured directly the partial molar mixing enthalpies of CaO, ΔH_{CaO}^{mix} , by the isothermal drop calorimeter. The partial molar mixing enthalpies were determined also from the enthalpy difference between the directly measured enthalpy $\Delta H^1 (T_K - T_0)$ and calculated enthalpy $\Delta H^2 (T_K - T_0)$ using a heat capacity of CaO [KNA 1991] with the following scheme:



The directly measured enthalpies ΔH^1 and the partial molar mixing enthalpies of CaO are listed in table 5.14.

Tab 5.14 Enthalpy increment ΔH^1_{CaO} measured by dropping CaO into the calorimeter from room temperature ($T_0 = 295$ K) to the calorimetric temperature ($T_K = 1732$ K) and the partial molar mixing enthalpies of CaO ΔH^{mix}_{CaO}

	ΔH^1_{CaO} [J/g] number of measurements(n)	ΔH^{mix}_{CaO} [J/g]
Sample A	976.2 ± 49 (5)	-381.6
Sample B	1043.5 ± 37 (6)	-314.3
Sample C	949.9 ± 47 (7)	-407.9
Sample D	645.3 ± 29 (9)	-712.5
Sample F	929.1 ± 44 (7)	-428.7
Sample G	816.7 ± 35 (10)	-541.1

As demonstrated in the preceding chapter, we calculated the partial molar mixing enthalpies of CaO by Gibbs-Helmholtz equation from the activities of CaO calculated by the constitutional model or $F^*A^*C^*T$. We compared the directly measured partial molar mixing enthalpies of CaO to the calculated values in table 5.15.

Tab 5.15 Partial molar mixing enthalpies of CaO at 1732 K.

Comparison of values $\Delta H^{mix}_{CaO}{}^1$, measured in this study with values $\Delta H^{mix}_{CaO}{}^2$, calculated from the constitutional model and $\Delta H^{mix}_{CaO}{}^3$, calculated from $F^*A^*C^*T$

	$\Delta H^{mix}_{CaO}{}^1$ [kJ/mol]	$\Delta H^{mix}_{CaO}{}^2$ [kJ/mol]	$\Delta H^{mix}_{CaO}{}^3$ [kJ/mol]
Sample A	-21.4	-42.8	-54.7
Sample B	-17.6	-22.8	-45.4
Sample C	-22.9	-7.6	-57.1
Sample D	-40.0	-42.6	-67.2
Sample F	-24.0	-23.1	-45.8
Sample G	-30.3	-8.2	-56.9

Partial molar mixing enthalpies can be determined indirectly by a method of tangential intercepts in a binary system. But an extension of this method to multicomponent systems is very difficult from the viewpoint of experiments. Therefore the direct, experimental method for the measurement of partial molar mixing enthalpies is thus necessary.

The comparison in table 5.15 shows that there is difference between the measured and the calculated by the constitutional model and by $F^*A^*C^*T$. Consider Gibbs energy changes for the mixing process. If, at constant T and P , x_i mole fraction of i are mixed to form a solution,

$$\text{the Gibbs energy before mixing} = \sum x_i \cdot G_i^0$$

and

$$\text{the Gibbs energy after mixing} = \sum x_i \cdot \bar{G}_i$$

where G_i^0 and \bar{G}_i denote the molar Gibbs energy of pure i and the partial molar Gibbs energy of i in the solution, respectively. The Gibbs energy change due to mixing, ΔG^{mix} , is the difference between these quantities; i.e.,

$$\Delta G^{\text{mix}} = \sum x_i (\bar{G}_i - G_i^0).$$

For the partial molar mixing energy of CaO

$$\Delta G_{\text{CaO}}^{\text{mix}} = \bar{G}_{\text{CaO}} - G_{\text{CaO}}^0 = \Delta H_{\text{CaO}}^{\text{mix}} - T \cdot \Delta S_{\text{CaO}}^{\text{mix}}.$$

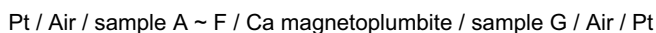
According to the literature data [KNA 1991], the molar Gibbs energy of CaO at 1732 K (G_{CaO}^0) is -781.3 kJ/mol. This value is about 30 times as much as the partial molar mixing enthalpy of CaO ($\Delta H_{\text{CaO}}^{\text{mix}}$).

If we consider the above fact, the difference between the measured and the calculated is not a surprising result. As described in the preceding chapter, partial molar mixing enthalpies of CaO, $\Delta H_{\text{CaO}}^{\text{mix}}$, were calculated by the Gibbs-Helmholtz equation from the activities of CaO calculated by the constitutional model or $F^*A^*C^*T$. Because activities used for the calculation of the partial molar mixing enthalpies are derivative properties, the accuracy of partial molar mixing enthalpies is however much poorer than that of calculated activities. Hence it is needless to say that the accuracy of the calculated partial molar mixing enthalpies of CaO by this method is lower than that of the direct measurements.

6 Summary

The purpose of the present investigation is to illustrate experimental methods for the measurement of accurate thermodynamic data in silicate glasses and melts, and then to determine thermochemical properties by those methods in order to improve the accuracy of models proposed for calculation in the multicomponent silicate system. Experimental thermochemical data served as a criterion for the reliability of statistical models and confirmed the possibility of experimental methods to use as tools in the multicomponent system. As experimental methods, electrochemical (EMF) and calorimetric (DSC, isothermal drop calorimeter) methods were used to determine thermochemical properties and as calculation procedure, the constitutional model and a commercial software F*A*C*T were adopted to compare the calculated values with the measured values. Thermochemical data for constitutional compounds were gathered to calculate thermodynamic properties from various data banks.

Activity of CaO in the silicate melts is determined by EMF method using calcium magnetoplumbite ($\text{CaO} \cdot 6\text{Al}_2\text{O}_3$) as solid electrolyte. Using sample G as reference, activities of CaO in other samples were measured with the following cell reaction:



The experimental activities of CaO were compared with the calculated values by the constitutional model and F*A*C*T, respectively. Except for sample D, the calculated values by two models are within ± 0.2 from the measured values as decadal logarithms with a good agreement.

Calcium β'' -alumina as solid electrolyte was prepared by two-step ion-exchange process from the commercial sodium β'' -alumina tubes. The EMF measured by partially ion-exchanged calcium β'' -alumina are compared with the literature values. By using equation 3.3, we determined an ionic transport number of CaO ($t_{\text{Ca}^{2+}}$) in the partially ion-exchanged calcium β'' -alumina.

$$E = - \frac{R \cdot T}{2 \cdot F} \cdot \int_{a_{CaO}^{right}}^{a_{CaO}^{left}} t_{Ca^{2+}} d \ln a_{CaO} . \quad (3.3)$$

The partial molar mixing enthalpies of CaO, ΔH_{CaO}^{mix} , were measured directly by the isothermal drop calorimeter with dropping CaO pellet into melts at 1732 K. The measured values were compared with the calculated values, which were derived with Gibbs-Helmholtz equation from the calculated CaO activities by the constitutional model and $F \cdot A \cdot C \cdot T$, respectively. The comparison shows a poor agreement between the measured and the calculated values, which is due to the fact that the Gibbs-Helmholtz equation relies on the T derivatives of measured data, which we usually burdened with a large error.

The vitrification enthalpy H^{vit} was measured by the isothermal drop calorimeter. The measurements for the vitrification enthalpy were carried out in the temperature range from room temperature T_0 (295 K) to the calorimetric temperature T_k (1732 K). Enthalpy data were determined from the enthalpy difference $\Delta H (T_k - T_0)$.

The melting enthalpies H^m are determined using equation 2.28 with the experimental measured values: H^{vit} from the drop calorimeter measurements and ΔC_p , T_g from the DSC measurements.

$$H^m - H^{vit} = \Delta C_p \cdot (T_{liq} - T_g) \quad (2.28)$$

The determined H^m and the experimental measured H^{vit} suggest $H^{vit} = (0.6 \pm 0.09) \cdot H^m$, which is in good agreement with the concept $H^{vit} \approx 0.6 H^m$, except for sample C.

The vitrification enthalpies H^{vit} calculated by the constitutional model are compared with the experimental determined values. The comparison showed that the values from the constitutional model agree well with those from the experiments. The oxide activities in the melts are also calculated by the constitutional model using equation 4.15 and 4.21. For the calculation of activities using the constitutional model, one needs to carefully choose the

concept applied, i.e., the nanoscale mixture (4.15) or the homogeneous mixture (4.21).

$$\ln a_j = \sum_k A_{jk} \cdot \left[\frac{G_k^0}{R \cdot T} \right] - \frac{G_j^0}{R \cdot T} \quad (4.15)$$

$$\ln a_j = \sum_k A_{jk} \cdot \left[\frac{G_k^0}{R \cdot T} + \ln x_k \right] - \frac{G_j^0}{R \cdot T} \quad (4.21)$$

For the calculation of oxide activities using the commercial software F*A*C*T, it is very important to note that the calculated oxide properties are related to the liquid state of oxide. By contrast properties from the constitutional model are related to the solid state of oxide. For the sake of comparison of two models, the reference state of oxide has to be considered.

7 References

- [ADA 1965] Adam, G.; J.H. Gibbs: On the temperature dependence of cooperative relaxation properties in glass-forming liquids. *J. Chem. Phys.* 43 (1965), 139-146
- [ADA 1980] K. Adamkovičová; L. Kosa; I. Proks: The heat of fusion of CaSiO_3 . *Silikaty* 24, 193-201, 1980
- [BAB 1985] V.I.Babushkin; G.M.Matveyev; O.P.Mchedlov-Petrosyan: *Thermodynamics of Silicates*. Springer, Berlin 1985
- [BAL 2002] C. W. Bale; P. Chartrand; S. A. Degterov; G. Eriksson; K. Hack; R. Ben Mahfoud; J. Melançon; A. D. Pelton; S. Petersen: Factsage thermochemical software and databases. *CALPHAD*, 26 (2002) 189-228
- [BAR 1972] Bartenev, G. M.; et al.: Molikularkinetische Prozesse in Schmelzen anorganischer Gläser im Transformationsbereich. *Silikattechnik* 23 (1972) 155-159
- [BLA 1983] M. Blander; A.D. Pelton: *Computer-Assisted Analyses of The Thermodynamic Properties of Slags in Coal-Combustion Systems*. Department of Metallurgical Engineering, Ecole Polytechnique, Uni. Of Montreal, Quebec. (1983).
- [BON 1990] D. W. Bonnel; J. W. Hastie: A Predictive Thermodynamic Model for complex High Temperature Solution Phases XI. *High Temp. Sci.* Vol. 26 (1990) 313-334
- [BOT 1978] Bottinga, Y.; P. Richet: Thermodynamics of liquid silicates, a preliminary report. *Earth Planet. Sci. Lett.*, 40, 382-400, 1978
- [BRO 1984] C. Brousse; R. C. Newton; O. J. Kleppa: Enthalpy of formation of forsterite, enstatite, akermanite, monticellite and merwinite at 1073 K determined by alkali borate solution calorimeter. *Geochimica et Cosmochimica Acta* Vol. 48, pp. 1081-1088, 1984
- [CAR 1977] Carmichael i. S.; Nicholls j.; Spera F. j.; Wood B. J.; Nelson S. A.: High temperature properties of silicate liquids: applications to the equilibration and ascent of basaltic magma. *Philos. Trans. R. Soc. London Ser. A.* 286 (1977), 373-431
- [CHA 1975] T. V. Charlus; R. C. Newton; O. J. Kleppa: Enthalpies of formation at 970 K of compounds in the system $\text{MgO-Al}_2\text{O}_3$ -

- SiO₂ from high temperature solution calorimeter. *Geochim. Cosmochim. Acta.* 1975. Vol. 39. pp 1487-1497
- [CHA 1978] T. V. Charlu; R. C. Newton; O. J. Kleppa: Enthalpy of formation of some lime silicates by high-temperature solution calorimeter, with discussion of high pressure phase equilibria. *Geochim. Cosmochim. Acta.* 1978, Vol. 42. pp. 367-375
- [CHA 1981] T. V. Charlu; R. C. Newton; O. J. Kleppa: Thermochemistry of synthetic Ca₂Al₂SiO₇ (gehlenite)-Ca₂MgSi₂O₇ (akermanite) melilites. *Geochimica et Cosmochimica Acta* Vol. 45, pp. 1609-1617, 1981
- [CHA 1983] Chatillon-Colinet C.; Newton R. C.; Perken D.; Kleppa O. J.: Thermochemistry of (Fe²⁺, Mg)SiO₃ orthopyroxene. *Geochim. Cosmochim. Acta* 47 (1983), 1597-1603.
- [CHA 1985] M. W. Jr. Chase ; C. A. Davies ; J. R. Jr. Downey; D. J. Frurip; R. A. McDonald; A. D. Syverud: *JANAF Thermochemical tables.* The American Ceramic Society, Michigan, 1985.
- [CHA 1998] Champagnon, B.; C. Chemarin; P. Richet: Fictive temperature and the medium range order in silicate glasses: a relationship between heat capacity and boson peak. *Phil. Mag.* B77 (1998), 663-669
- [CON 1995] Conradt R.: A thermodynamic approach to multicomponent oxide glasses. *Glastech. Ber. Glass Sci. Technol.* 68C1 (1995) 43-50
- [CON 1997] Conradt R.: A thermodynamic approach to the structure of oxide glasses. *Fundamentals of Glass Science and Technology* (1997)
- [CON 1998] Conradt R.: A simplified procedure to estimate thermodynamic activities in multicomponent oxide melts. *Molten Salt Forum*, vol. 5-6 (1998) 155-162.
- [CON 1999*] Conradt R.: Thermochemical methods in glass technology. 13th conference on glass and ceramics, proceedings vol. 1 glass (1999)
- [CON 1999] Conradt R.: Thermochemistry and structure of oxide glasses, Bach H. and Krause (eds.) *Analysis of the composition and structure of glass and glass ceramics*, Springer Verlag, Berlin (1999) 232-254.

- [CON 2000] R. Conradt: A quantitative approach to the properties of geological and industrial glass forming systems. Applied Mineralogy. 115-118, 2000
- [CON 2004] R. Conradt: CHEMICAL STRUCTURE, MEDIUM RANGE ORDER, AND CRYSTALLINE REFERENCE STATE OF MULTICOMPONENT OXIDE LIQUIDS AND GLASSES. X. Int. Conf. on Physics of Non-Crystalline Solids, July 13-17, 2003, Parma, Italy, accepted for publishing in Journal of Non-Crystalline Solids 2004.
- [COU 1993] Courtial P.; Richet P.: Heat capacity of magnesium aluminosilicate melts. *Geochimica et Cosmochimica Acta*, 57 (1993), 1267-1275
- [DUN 1980] Dunn B.; Farrington G. C.; Fast divalent ion conduction in Ba⁺⁺, Cd⁺⁺ and Sr⁺⁺ β" aluminas. *Mat. Res. Bull.*, Vol. 15, pp. 1773-1777, 1980.
- [FER 1971] Ferrier A.: Etude experimentale de L'Enthalpie Cristallisation du Diopside et de L'Anorthite Synthetis que. *Rev. Int. Hautes Temp. Refract.* 8 (1971), 31-36
- [FRA 1993] D.J. Fray; R.V. Kumar: Electrochemical determination of the thermodynamics of the Ca-Pb system at 1173K using calcium magnetoplumbite as the electrolyte. *Scandinavian Journal of Metallurgy* 1993, 22. 266-270
- [GAY 1984] Gaye, H., in: H. Gay, D. Colombet(eds.), *Données thermochimiques et cinétiques relatives à certains matériaux sidérurgiques*, Commission de la Communautés Européennes Convention CECC No. 7210-CF/301 TCM-RE 1064, Mars (1984).
- [GLA 1990] Horst Scholze: *Glass. Nature, Structure, and Properties*. Springer-Verlag
- [GUT 1995] Gutzow I.; J. Schmelzer: *The Vitreous State*. Springer Verlag, Berlin, 1995
- [HEM 1977] Hemley J. J.; Montoya J. W.; Shaw D. R.; Luce R. W.: Mineral equilibria in the MgO-SiO₂-H₂O system: Talc-antigorite-forsterite-anthophyllite-enstatite stability relations and some geologic implications in the system. *Amer. J. Sci.* 277 (1977b), 353-383.
- [HEL 1978] Helgeson H. C.; Delany J. M.; Nesbitt H. W.; Bird D. K.: Summary and critique of the thermodynamic properties of rock-forming minerals. *Amer. J. Sci.* 278-A (1978), 1-229

- [HER 1984] Hervig, R. L.; Navrotsky A.: Thermochemical study of glasses in the system $\text{NaAlSi}_3\text{O}_8$ - KAlSi_3O_8 - Si_4O_8 and the join $\text{Na}_{1.6}\text{Al}_{1.6}\text{Si}_{2.4}\text{O}_8$ - $\text{K}_{1.6}\text{Al}_{1.6}\text{Si}_{2.4}\text{O}_8$. *Geochim. Cosmochim. Acta*, 48, 513-522, 1984
- [HER 1985] Hervig, R. L.; D. Scott; A. Navrotsky: Thermochemistry of glasses along joins of pyroxene stoichiometry in the system $\text{Ca}_2\text{Si}_2\text{O}_6$ - $\text{Mg}_2\text{Si}_2\text{O}_6$ - Al_4O_6 . *Geochim. Cosmochim. Acta*, 49, 1487-1492, 1985
- [HON 1987] Hong Y.; Hong D.; Peng Y.; Li L.; Wei S.: The fabrication and properties of polycrystalline $\text{Ca} \beta$ - Al_2O_3 tube. *Solid State Ionics*, 1987: 25: 301-305
- [HOL 1967] Holm J. L.; Kleppa O. J.; Westrum E. F. Jr: Thermodynamics of polymorphic transformations in silica. Thermal properties from 5 to 1070 °K and pressure temperature stability fields for coesite and stishovite. *Geochim. Cosmochim. Acta* 31 (1967), 2289-2307
- [KIN 1967] King E. G.; Barany R.; Weller W. W.: Thermodynamic properties of forsterite and serpentine. U.S. Bur. of Mines Rept. Invest. 6962, 1967
- [KIR 1991] Kirchenerova J.; Petric A.; Bale C. W.; Pelton A. D.: Dense polycrystalline calcium β - and β -aluminas: synthesis, XRD characterization and thermal stability. *Mat. Res. Bull.*, Vol. 26, pp. 527-534, 1991
- [KIS 1979] I. A. Kiseleva; L. P. Ogorodova; N. D. Topor; O. G. Chigareva: A thermochemical study of the CaO-MgO-SiO_2 system. *Geokhimiya* 12, 1811-1825, 1979
- [KNA 1991] O. Knacke; O. Kubaschewski; K. Hesselmann: Thermochemical Properties of Inorganic Substances. Second Edition (1991), Springer Verlag, Düsseldorf
- [KOC 1975] K. Koch; G. Toemel; G. Heinz: Das Zustandsdiagramm Al_2O_3 - CaO-MgO-SiO_2 in polythermischer Darstellung. *Tonind.-Ztg. Keram. Rundschau* 99 (1975) 3 p. 57-62 (Phasediagrams for Ceramists fig. 5476).
- [KRA 1953] Kracek F. C.: Contributions of thermochemical and X-ray data to the problem of mineral stability. *Carnegy Inst. Washington Yearb.* 52, 69-75, 1953
- [KUM 1985] Kumar R. V.; Kay D. A. R.: The utilization of galvanic cells using $\text{Ca} \beta$ -Alumina solid electrolytes in a thermodynamic

- investigation of the CaO-Al₂O₃ system. *Met. Trans. B*, Vol. 16B: 107, 1985
- [LAN 1991] Rebecca A. Lange; James J. De Yoreo; Alexandra Navrotsky: Scanning calorimetric measurement of heat capacity during incongruent melting of Diopside. *American Mineralogist*, Vol. 76, pages 904-912, 1991
- [LEV 1964] Levin, E. M.; C. R. Robbins; H. F. McMurdie: *Phase Diagrams for Ceramists*. 2nd ed., 601 pp., American Ceramic Society, Columbus, Ohio, 1964.
- [MAC 1960] Mackenzie J. D.: *Modern Aspects of the Vitreous State*. Butterworth, London, Vol. 1 (1960), Vol. 2 (1962), Vol. 3 (1964).
- [NAV 1971] Navrotsky A.: Thermodynamics of formation of the silicates and germinates of some divalent transition metals and of magnesium. *J. Inorg. Nucl. Chem.* 33 (1971), 4033-4050
- [NAV 1976] Navrotsky A.; Coons W. E.: Thermochemicals of some pyroxenes and related compounds. *Geochim. Cosmochim. Acta* 40 (1976), 1281-1288
- [NAV 1980] A. Navrotsky; R. Hon; D. F. Weill; D. J. Henry: Thermochemistry of glasses and liquids in the systems CaMgSi₂O₆-CaAl₂Si₂O₈-NaAlSi₃O₈, SiO₂-CaAl₂Si₂O₈-NaAlSi₃O₈ and SiO₂-Al₂O₃-CaO-Na₂O. *Geochim. Cosmochim. Acta* 44, 1409-1423, 1980.
- [NEW] R. C. Newton; A. Navrotsky; B. J. Wood: *Thermodynamics of Minerals and Melts*
- [NEU 1952] Neuvonen K. J.: Thermochemical investigation of the akermanite-gehlenite series. *Bull. Comm. Geol. Finl.*, 158, 50 pp., 1952
- [NEW 1979] Newton R. C.; Charlu T. V.; Anderson P. A. M.; Kleppa O. J.: "Thermochemistry of synthetic clinopyroxenes on the join CaMgSi₂O₆-Mg₂Si₂O₆. *Geochim. Cosmochim. Acta* 43 (1979), 55-60
- [NEW 1980] R. C. Newton; T. V. Charlu; O. J. Kleppa: Thermochemistry of the high structural state plagioclases. *Geochimica et Cosmochimica Acta* Vol. 44 (1980), pp. 933-941
- [ORS 1975] Orsini P. G.; A. Buri; A. Marotta: Devitrification of glasses in the akermanite-gehlenite system. *J. Am. Chem.*, 8, 78-82, 1969

- [PEL 1986] A. D. Pelton; M. Blander: Thermodynamic Analysis of Ordered Liquid Solutions by a Modified Quasichemical Approach-Application to Silicate Slags. *Met. Trans. B*, 17B (1986) 805-815
- [PHA 1998] Phase equilibria diagrams: CD-ROM databases. The American Ceramic Society, Westerville, Ohio, (1998).
- [PHI 1990] Philpotts A. R.: Principles of igneous and metamorphic petrology. Prentice Hall, Englewood Cliffs, New Jersey, (1990).
- [PLU 1966] E. Plumat; F. Toussanit; M. Boffe; Formation of Bubbles by Electrochemical Processes in Glass. *J. Am. Ceram. Soc.* 49 (1966) 551.
- [PRO 1977] Proks I.; M. Eliášová; L. Kosa: The heat of fusion of akermanite. *Silikaty Prague*, 21, 3-11, 1977.
- [ROB 1978] Richard A. Robie; Bruce S. Hemingway; James R. Fisher: Thermodynamic properties of minerals and related substances at 298.15 K and 1 Bar (10^5 Pascals) Pressure and at Higher Temperatures. United States Government printing office, Washington, 1978
- [ROG 1974] Rog G.; Langanke B.; Borchardt G.; Schmalzied H.: Determination of the standard Gibbs free energies of formation of the silicates of cobalt, magnesium, and strontium by e.m.f. measurements. *J. Chem. Thermo.* 6 (1974), 1113-1119
- [ROG 1993] G. Róg; A. Kozłowska-Róg; K. Zakula-Sokół: Determination of the standard gibbs free energies of formation of the calcium aluminates from the oxides by e.m.f. measurements. *J. Chem. Thermodynamics* 1993, 25, 807-810
- [RIC 1982] Richet P.; Bottinga Y.: Models for the calculation of heat capacity of glassy and liquid silicates. *C. R. Hebd. Seances Acad. Sci., Ser. 2*, 295, 1121-1124, 1982
- [RIC 1984] P. Richet; Y. Bottinga: anorthite, andesine, wollastonite, diopside, cordierite and pyrope: glass transitions, thermodynamics of melting, and properties of the amorphous phases. *Earth Planet. Sci. Lett.*, 67, 415-432, 1984
- [RIC 1986] Pascal Richet: Thermochemical Properties of Silicate Glasses and Liquids: A Review. *Reviews of geophysics*, vol. 24, No. 1, Pages 1-25, February 1986
- [RIC 1993] Richet P.; Leclerc F.; Benoist L.: Melting of forsterite and spinel, with implications for the glass transition of Mg_2SiO_4 liquid. *Geophysical Research Letters*, 20 (1993a), 1675-1678

- [RIC 1994] Pascal Richet; Janick Ingrin; Bjorn O. Mysen; Philippe Courtial; Philippe Gillet: Premelting effects in minerals: an experimental study. *Earth and Planetary Science Letters* 121 (1994) 589-600
- [SCH 1990] Schaefer GW, Van Zyl, A Weppner W.: Direct synthesis of divalent β -alumina and related phases. *Solid State Ionics* 1990: 40/41: 154-157
- [SER 1995] Sergei V. Nemilov: *Thermodynamic and Kinetic Aspects of the Vitreous State*. 1995
- [SHE 1973] Shearer J. A.; Kleppa O. J.: The enthalpies of formation of $MgAl_2O_4$, $MgSiO_3$, Mg_2SiO_4 and Al_2SiO_5 by oxide melt solution calorimeter. *J. Inorg. Nucl. Chem.* 35 (1973), 1073-1078
- [STE 1984] Stebbins J. F.; I. S. E. Carmichael; L. K. Moret: Heat capacities and entropies of silicate liquids and glasses. *Contrib. Mineral. Petrol.*, 86, 131-148, 1984
- [STE 1995] J. F. Stebbins; P. F. McMillan; D. B. Dingwell: *Structure, Dynamics and Properties of Silicate Melts*. *Reviews in Mineralogy* Volume 32, 1995
- [SUB 1980] E. C. Subbarao: *Solid Electrolytes and Their Applications*. 1980 Plenum press, New York
- [TAN 1996] Jun Tanabe; Kazuhiro Nagata: Use of Solid-Electrolyte Galvanic Cells to Determine the Activity of CaO in the CaO-ZrO₂ System and the Standard Gibbs Free Energies of Formation of CaZrO₃ from CaO and ZrO₂. *Metallurgical and Materials transactions B* (1996), Vol. 27B, 658-662
- [TAR 1994] Igor Tarina; Alexandra Navrotsky; Hao Gan: Direct calorimetric measurement of enthalpies in diopside-anorthite-wollastonite. *Geochimica et Cosmochimica Acta*, Vol.58, No.17, pp.3665-3673, 1994
- [THO 1988] W. T. Thompson; A. D. Pelton; C. W. Bade: *F*A*C*T facility for the analysis of chemical thermodynamics. Guide to operations*. Mc Gill Univ., Montreal, 1988.
- [TOR 1948] Torgesen D. R.; Sahama Th. G.: A hydrofluoric acid solution calorimeter and the determinations of the heats of formation of Mg_2SiO_4 , $MgSiO_3$, and $CaSiO_3$. *J. Amer. Chem. Soc.* 70 (1948), 2156-2160
- [UBB 1965] Ubbelohde A. R.: *Melting and Crystal Structure*. Clarendon, Oxford, (1965).

- [WAG 1933] C. Wagner: Beitrag zur Theorie des Anlaufvorgangs. Zeitschrift für Phys. Chem. B 21 (1933). 25-41
- [WAG 1966] C. Wagner: Advances of Electrochemistry and Electrochemical Engineering. Vol. 4, ed. P. Delahay, Interscience, New York (1966), p. 2.
- [WEB 2001] Richard Weber; Jean Tangeman; Thomas Key; Paul Nordine: Synthesis and structure of an orthosilicate glass: Mg_2SiO_4 . Proc. Int. Congr. Glass, Volume 2. Extended Abstracts, Edinburgh, Scotland, 1-6 July 2001
- [WEI 1980] Weill D. F.; Hon R.; Navrotsky A.: The igneous system $CaMgSi_2O_6$ - $CaAl_2Si_2O_8$ - $NaAlSi_3O_8$: variations on a classic theme by Bowen. In Physics of Magmatic Processes (ed. R. B. Hargraves) Princeton Univ. Press, 1980
- [WHI 1985] Whiter J. T.; Fray D. J.: The preparation and electrical properties of polycrystalline calcium β "-alumina. Solid State Ionics 17 (1985), 1-6
- [WIL 1989] W. Wilsmann; F. Müller: Design and characteristics of a differential calorimeter for high-temperature measurements. Thermochemica Acta, 151 (1989) 309-318
- [YOD 1976] Yoder H. S.: Generation of Basaltic Magmas. p. 91. National Academy of Sciences, Washington, 1976
- [ZWI 2001] 2. Zwischenbericht zum Forschungsvorgaben CO 249/1-2, Deutsche Forschungsgemeinschaft, (2001)
- [ZAR 1991] J. Zarzycki: Glasses and the vitreous state. Cambridge Solid State Science Series. 1991
- [ZEN 1976] Zen e.-A.; Chernosky J. V.: Correlated free energy values of anthophyllite, brucite, clinocrosotile, enstatite, forsterite, quartz, and talc. Amer. Mineral. 61 (1976), 1156-1166.

8 Appendices

8.1 Data for constitutional compounds

CAS₂ (Anorthite)

H ^m in kJ/mol	H ^{lit} in kJ/mol	T _g in K	T ^m in K	C _{ps} J/mol K	C _{pl} J/mol K	Reference
136	77.8		1830			WEI 1980
132.7	78.2		1830			YOD 1976
166.9	103		1830			FER 1971
	71.8					KRA 1953
133		1160	1830			RIC 1984
146	103	1113	1826			CON 1999
166.9			1826	$297.022+43.388*10^{-3}T-13.535*10^6T^{-2}$	397.48	KNA 1991
	81		1830	$5.1683*10^2-9.2492*10^2T+4.1883*10^{-5}T^2-4.5885*10^3T^{-0.5}-1.4085*10^6T^{-2}$		ROB 1978
123			1823	$269.5+57.3*10^{-3}T-70.67*10^5T^{-2}$		BAB 1985
		1120	1830			SER 1995
		1109				STE 1995

CMS₂ (Diopside)

H ^m in kJ/mol	H ^{lit} in kJ/mol	T _g in K	T ^m in K	C _{ps} J/mol K	C _{pl} J/mol K	Reference
142.6	85.6		1665			WEI 1980
138.6	87.9		1670			NAV 1976
	77.4					YOD 1976
128.4	93		1665			FER 1971
	92.4					KRA 1953
138.2	86.4		1670			KIS 1979
129.9			1665			CAR 1977
136.4	85.6		1670			NAV 1980
137.7			1665			LAN 1991
137.7			1670			RIC 1994
128.4	92.3	981	1665			CON 1999
128.4			1665	$186.021+123.763*10^{-3}T-5.59*10^6T^{-2}-43.932*10^6T^2$		KNA 1991
77.40			1665	$1.9182*10^2+8.3079*10^2T-2.1718*10^{-5}T^2-4.2795*10^6T^{-2}$		ROB 1978
96.23			1665	$221.2+32.8*10^{-3}T-65.86*10^5T^{-2}$		BAB 1985
		973				STE 1995
		1005			33.46	RIC 1984

C₂MS₂ (Akermanite)

H ^m in kJ/mol	H ^{vit} in kJ/mol	T _g in K	T ^m in K	C _{ps} J/mol K	C _{pl} J/mol K	Reference
123.9			1727			PRO 1977
114.8	32.5		1727			NEU 1952
124.6			1727			RIC 1994
165.7	106.7	1036	1727			CON 1999
			1727	$251.96+47.237*10^{-3}T-4.803*10^6T^{-2}$		KNA 1991
			1727	$4.4511*10^{-2}-5.1463*10^{-2}T+2.1857*10^{-5}T^2-3.7937*10^{-3}T^{0.5}$		ROB 1978
165.7			1727			BAB 1985

M₂S (Forsterite)

H ^m in kJ/mol	H ^{vit} in kJ/mol	T _g in K	T ^m in K	C _{ps} J/mol K	C _{pl} J/mol K	reference
71		990	2174		252.9	RIC 1993
	61.44					WEB 2001
71.1	42.7	1298	2163			CON 1999
71.1			2171	$144.306+38.744*10^{-3}T-3.284*10^6T^{-2}-5.481*10^{-6}T^2$		KNA 1991
			2163	$2.2798*10^{-2}+3.4139*10^{-3}T-1.7446*10^{-5}T^{0.5}-8.9397*10^{-5}T^{-2}$		ROB 1978
105.4			2163	$149.8+27.36*10^{-3}T-35.65*10^5T^{-2}$		BAB 1985
121.3			1890			NEW

CS (Pseudowollastonite)

H ^m in kJ/mol	H ^{vit} in kJ/mol	T _g in K	T ^m in K	C _{ps} J/mol K	C _{pl} J/mol K	reference
	29.9					ADA 1980
	25.4					HER 1985
57.3			1817			ADA 1980
55			1817			HER 1985
57			1827			TAR 1994
57.3			1821			RIC 1994
82.8	49.8	1065	1817			CON 1999
27.405				$1.0710*10^{-2}+1.7481*10^{-2}T-2.2965*10^6T^{-2}$		ROB 1978
59.831			1813	$108.2+16.5*10^{-3}T-23.6*10^5T^{-2}$		BAB 1985
		1065				STE 1995

MS (Enstatite)

H ^m in kJ/mol	H ^{lit} in kJ/mol	T _g in K	T ^m in K	C _{ps} J/mol K	C _{pl} J/mol K	Reference
73.2	42.15		1834			HER 1985
77.4			1834			STE 1984
73.2			1834			RIC 1986
72.68						HER 1985
71.96						NEW 1979
73.47						CHA 1975
		1056			167.2	COU 1993
75.3	46.6	1110	1850			CON 1999
75.3			1850	92.048+33.054*10 ⁻³ T- 1.778*10 ⁶ T ⁻² (< 903 K) 120.332 (< 1258 K) 122.424 (< 1850 K)	146.44	KNA 1991
61.51			1830	2.0556*10 ⁻² -1.2796*10 ⁻² T- 2.2977*10 ³ T ^{-0.5} +1.1926*10 ⁶ T ⁻²		ROB 1978
61.51			1797	102.72+19.83*10 ⁻³ T- 26.28*10 ⁵ T ⁻²		BAB 1985
		874				STE 1995

C₂AS (Gehlenite)

H ^m in kJ/mol	H ^{lit} in kJ/mol	T _g in K	T ^m in K	C _{ps} J/mol K	C _{pl} J/mol K	reference
	49.8					NEU 1952
			1866			LEV 1964
		1133				ORS 1975
216.2	129.9	1118	1863			CON 1999
			1863	275+27.907*10 ⁻³ T- 7.82*10 ⁶ T ⁻²		KNA 1991
			1863	4.0513*10 ⁻² -7.0986*10 ⁻³ T- 3.1744*10 ³ T ^{-0.5} -1.1883*10 ⁶ T ⁻²		ROB 1978
				266.5+33.472*10 ⁻³ T- 63.18*10 ⁵ T ⁻²		BAB 1985

S (Cristobalite)

H ^m in kJ/mol	H ^{lit} in kJ/mol	T _g in K	T ^m in K	C _{ps} J/mol K	C _{pl} J/molK	reference
	6.1					WEI 1980
8.16	4.6		1996			HOL 1967
	3.9					ROB 1978
8.92			1999			RIC 1982
9.6	6.9	1495	1996			CON 1999
9.581			2001	46.903+31.506*10 ⁻³ T- 1.008*10 ⁶ T ⁻² (< 543 K) 71.63+1.883*10 ⁻³ T- 3.908*10 ⁶ T ⁻² (< 1079 K) 71.63+1.883*10 ⁻³ T- 3.908*10 ⁶ T ⁻² (< 2001 K)	85.772	KNA 1991
8.159			1996	-4.1596*10 ³ +2.5480*T +7.1680*10 ⁴ T ^{-0.5} -6.2859 *10 ⁷ T ⁻² (< 523 K) 72.753+1.3004*10 ⁻³ T- 4.1320*10 ⁶ T ⁻² (< 1800 K)		ROB 1978
9.205			1713	55.98+15.4*10 ⁻³ T- 14.43*10 ⁵ T ⁻²		BAB 1985
8.159	4.602		1996			NEW
10.45		1450	1998			SER 1995
14.3	10.5	1473	1996			GUT 1995
9.1	5.6					GUT 1995
		1480				STE 1995

8.2 Formation enthalpy of constitutional compounds

CAS₂ (anorthite)

$\Delta H_{\text{ox}}^{\text{f}}$ (J/mol)	T in K	Reference
-96817	970	CHA 1978
-100123	970	CHA 1978
-91504	298	CHA 1978
-94475	970	CHA 1978
-100667	970	NEW 1980
-91211	298	KNA 1991
-110851	298	ROB 1978

C₂MS₂ (akermanite)

$\Delta H_{\text{ox}}^{\text{f}}$ (J/mol)	T in K	Reference
-179577	970	CHA 1981
-178238	1073	BRO 1984
-178238	1000	BRO 1984
-171962	298	BRO 1984
-183678	298	KNA 1991
-183452	298	ROB 1978

M₂S (forsterite)

$\Delta H_{\text{ox}}^{\text{f}}$ (J/mol)	T in K	Reference
-62634	970	CHA 1975
-60250	298	CHA 1975
-63262	298	TOR 1948
-57990	298	KIN 1967
-61630	298	NAV 1971
-59748	298	ROG 1974
-61505	298	CHA 1975
-61714	298	HEM 1977
-62258	298	HEL 1978
-58199	298	KIS 1979
-57823	298	BRO 1984
-59873	1000	BRO 1984
-59538	1073	BRO 1984
-63597	298	KNA 1991
-56690	298	ROB 1978

CMS₂ (diopside)

$\Delta H_{\text{ox}}^{\text{f}}$ (J/mol)	T in K	Reference
-146398	970	CHA 1978
-143051	298	CHA 1978
-145185	298	KNA 1991
-152781	298	ROB 1978

MS (enstatite)

$\Delta H_{\text{ox}}^{\text{f}}$ (J/mol)	T in K	Reference
-36861	970	CHA 1975
-35731	298	TOR 1948
-35731	298	SHE 1973
-37028	298	ROG 1974
-36903	298	HEM 1977
-32384	298	ZEN 1976
-34183	298	KIS 1979
-35982	298	CHA 1983
-33932	298	BRO 1984
-33890	1000	BRO 1984
-33890	1073	BRO 1984
-36401	298	KNA 1991
-35560	298	ROB 1978

CS (Pseudowollastonite)

$\Delta H_{\text{ox}}^{\text{f}}$ (J/mol)	T in K	Reference
-83345	970	CHA 1978
-81086	298	CHA 1978
-82861	298	ROB 1978

C₂AS (gehlenite)

$\Delta H_{\text{ox}}^{\text{f}}$ (J/mol)	T in K	Reference
-128198	970	CHA 1981
-132633	298	KNA 1991
-150992	298	ROB 1978

LEBENS LAUF

Persönliches

Jin-Wook Shin

geboren am 18.11.1970 in Yechon/ Korea

Eltern : Lehrer Hyoun-Du Shin und

Lehrerin Jeong-Ae Kim

verheiratet seit dem 15.09.2001 mit Hye-Jin Shin, geb. In

Schulbildung

1977-1983

Taeduk Grundschule, Taegu

1983-1986

Kyungsang Mittelschule, Taegu

1986-1989

Kyungsin Gymnasium, Taegu

Abschluss: Abitur

Studium

März 1989 –

Metallurgical Engineering

Februar 1996

Kyungpook National University

Abschluss: Bachelor of Engineering

Wehrdienst:

Januar 1990 - Juni 1992

März 1996-

Metallurgical Engineering

Februar 1998

Seoul National University

Abschluss: Master of Science in Engineering

Juli1998-Oktober1999

Deutschsprachkurse

an der Universität Gesamthochschule Essen

Abschluss: Deutsche Sprachprüfung für den Hochschulzugang

Oktober 1999-März 2000

Maschinenbau

Ruhr-Universität Bochum

seit Juli 2000

Promotion bei Prof. Dr. rer. nat. Reinhard Conradt,

im Institut für Gesteinshüttenkunde der RWTH, Lehrstuhl für Glas und

keramische Verbundwerkstoffe

29.06.04

Tag der mündlichen Prüfung

Berufstätigkeit

Juli 2000- Juni 2004

Wissenschaftlicher Mitarbeiter bei Prof. Dr. rer. nat. R. Conradt

im Institut für Gesteinshüttenkunde der RWTH Aachen.